

# Normalising Flow-based Differentiable Particle Filters

Xiongjie Chen and Yunpeng Li

**Abstract**—Recently, there has been a surge of interest in incorporating neural networks into particle filters, e.g. differentiable particle filters, to perform joint sequential state estimation and model learning for non-linear non-Gaussian state-space models in complex environments. Existing differentiable particle filters are mostly constructed with vanilla neural networks that do not allow density estimation. As a result, they are either restricted to a bootstrap particle filtering framework or employ predefined distribution families (e.g. Gaussian distributions), limiting their performance in more complex real-world scenarios. In this paper we present a differentiable particle filtering framework that uses (conditional) normalising flows to build its dynamic model, proposal distribution, and measurement model. This not only enables valid probability densities but also allows the proposed method to adaptively learn these modules in a flexible way, without being restricted to predefined distribution families. We derive the theoretical properties of the proposed filters and evaluate the proposed normalising flow-based differentiable particle filters’ performance through a series of numerical experiments.

**Index Terms**—Sequential Monte Carlo, Differentiable Particle Filters, Normalising Flows, Parameter Estimation, Machine Learning.

## I. INTRODUCTION

Particle filters, also known as sequential Monte Carlo (SMC) methods, are a class of importance sampling-based methods developed for performing sequential state estimation tasks in state-space models [1]–[3]. Because particle filters do not assume the linearity or Gaussianity on the considered state-space model and produce consistent estimators [4]–[8], they are particularly suitable for solving non-linear non-Gaussian filtering problems and have been widely adopted in various domains [9]–[12].

In cases where the state-space model of interest is known, particle filters can provide reliable approximations to posterior distributions of latent states. Since the celebrated bootstrap particle filter (BPF) was proposed [2], a series of particle filtering algorithms have been developed. For instance, the auxiliary particle filter (APF) improves its sampling efficiency by employing an auxiliary variable, such that the particles that are more compatible with the next observation have higher chances of survival [13]–[15]. The variance of the Monte Carlo estimates is reduced in the Rao-Blackwellised particle filter (RBPF) by marginalising out some latent states analytically [16], [17]. We refer readers to [1], [18], [19] for more detailed discussions of the above and several other variants of particle filtering methods, such as the unscented

particle filter [20], [21], the regularised particle filter [22], [23], the multiple particle filter [24], [25], and the Gaussian sum particle filter [26], [27].

In many real-world applications, parameters in the state-space model of interest are often unknown. Several techniques have been proposed to estimate the parameters in the state-space model [28], [29], among which maximum likelihood estimation methods and Bayesian estimation methods are the two main approaches in this direction. In maximum likelihood methods [30]–[32], estimates of the unknown parameters are obtained by searching for parameters that maximise the likelihood of observations given the estimate. In contrast, Bayesian estimation methods aim to estimate the posterior of parameters given observations through a specified prior distribution on the estimated parameters and the conditional likelihood of observations given parameters [33], [34]. In addition, depending on whether the observations are from fixed datasets or streaming dataflows, both Bayesian estimation and maximum likelihood estimation methods can be further divided into off-line and on-line methods [5], [35]–[38].

These parameter estimation methods have shown their effectiveness in certain scenarios, e.g. where the structure or a part of the parameters of the state-space model is known. Complex real-world cases require the learning of a full, complex state-space model from data. Recently, an emerging class of particle filters, often named differentiable particle filters (DPFs) [39]–[45], has received a surge of interest. Compared with classical parameter estimation techniques developed for particle filters, differentiable particle filters often make much less restrictive assumptions about the considered state-space model. Such flexibility makes them a promising tool for solving filtering tasks with complex high-dimensional environments, where the observations can be high-dimensional unstructured data such as images [40]–[42].

Components of differentiable particle filters, including dynamic models, measurement models, and proposal distributions, are mostly constructed with neural networks and optimised through gradient descent [40], [41], [46]–[48]. In [40], [41], it is assumed that the ground-truth latent states are accessible and neural networks employed in building differentiable particle filters are optimised by minimising supervised losses. By deriving an evidence lower bound (ELBO) of the observation log-likelihoods for filtering problems, unsupervised losses for training differentiable particle filters were proposed [46]–[48]. In a series of follow-up works [42], [43], [45], different differentiable resampling techniques and loss functions have been developed to achieve fully differentiable particle filters. It was investigated in [44] the impact of different design choices

X. Chen and Y. Li are with the Computer Science Research Centre, University of Surrey, Guildford GU2 7XH, U.K. (email: xiongjie.chen@surrey.ac.uk; yunpeng.li@surrey.ac.uk).

of dynamic models, measurement models, noise models, loss functions, and resampling schemes on the performance of differentiable particle filters. A detailed discussion of previous work that is most relevant to the proposed work is presented in Section I-A.

One limitation of existing differentiable particle filters is that most of them only employ vanilla neural networks to construct their components [40]–[42]. However, as vanilla neural networks do not allow density estimation, i.e. we do not know the probability density of their outputs, differentiable particle filters built with vanilla neural networks often include multiple levels of approximations such that desired statistical properties of standard particle filtering framework do not apply to these methods. For example, the transition density of particles is either modelled by simple distributions such as Gaussian distributions [41], [42] or ignored [40]. As a result, for all but a few trivial low-dimensional examples, existing differentiable particle filters are often restricted to the bootstrap particle filtering framework, making them susceptible to the weight degeneracy issue [49].

To address these issues, in this paper, we present a normalising flow-based differentiable particle filtering framework. By leveraging (conditional) normalising flows, the proposed method provides a flexible mechanism to model complex dynamics of latent states and design valid and effective proposal distributions. In addition, we use conditional normalising flows to construct measurement models that admit valid probability densities. The contributions of this paper are as follows:

- We propose a normalising flow-based differentiable particle filter (NF-DPF), which provides a flexible mechanism for modelling complex state-space models and admits valid probability densities for each component of the proposed method;
- We establish convergence results for the proposed method, proving that the approximation error of the resulting Monte Carlo estimates vanishes when the number of particles approaches infinity; To the best of our knowledge, this is the first work that established such convergence properties for both predictive and posterior approximations in differentiable particle filters.
- We report that the proposed method leads to improved performance over state-of-the-art differentiable particle filters on a variety of benchmark datasets in this field.

Some of our initial explorations on building differentiable particle filters with normalising flows were reported in abbreviated forms in conference papers [50], [51]. In this paper, more details of the proposed method are presented and discussed. Additionally, in this work, we establish convergence results for the proposed method and validate the effectiveness of the proposed method on a more extensive set of numerical experiments.

The rest of this paper is organised as follows. A detailed review of previous work relevant to our work is presented in Section I-A. The problem statement is presented in Section II. In Section III, we provide the necessary background knowledge for introducing the proposed method. The proposed normalising flow-based differentiable particle filter is detailed in Section IV. Convergence results of the proposed method

are established in Section V. The performance of the proposed method is evaluated and compared with the other differentiable particle filters in Section VI. We conclude this paper in Section VII.

#### A. Related Work

Parameter estimation for particle filters has long been an active research area, and various techniques have been proposed to address this task in several different directions [28], [29]. One type of such parameter estimation methods is the maximum likelihood (ML) methods [30]–[33], [52]–[56]. For off-line ML estimation, importance sampling and common random numbers methods are used in [32] and [30] respectively to create a continuous version of the resampling step and learn parameters of particle filters by maximising the marginal observation likelihood with gradient descent. To obtain a low-variance estimate of the gradient of log-likelihood, different variance reduction techniques have been proposed [31], [52]. An alternative approach that can maximise the log-likelihood in a numerically more stable way is the expectation-maximisation (EM) algorithm [33], [53], [54]. Both the gradient-based and the EM methods have their on-line variants to deal with very long observation sequences [55], [56]. Unlike off-line ML methods which require one to inspect the whole static dataset, on-line ML methods recursively update parameter estimates when new observations arrive.

In Bayesian parameter estimation methods, the parameters to be estimated are assigned with a prior distribution and the estimate is characterised by the posterior distribution of the parameters given the observations [5], [35]–[38], [57]–[60]. One typical example of off-line Bayesian parameter estimation method is the particle Markov chain Monte Carlo (PMCMC) method and its variants [35], [38], [60], which use Markov chain Monte Carlo (MCMC) samplers to generate Monte Carlo estimates of the parameter posterior. One approach to realise on-line parameter estimation in particle filters is to augment the state with the parameters. However, it was shown in [61] that the asymptotic variance of the resulting particle estimates diverges at least at a polynomial rate w.r.t. the dimension of the parameters. The SMC<sup>2</sup> algorithm [36] is an on-line method with variable cost per iteration. It consists of two layers of particle filters used to track the posterior of model parameters and latent variables simultaneously. In a similar nested hybrid filtering framework, nested particle filters were proposed within a purely recursive structure [37], [57], [58]. An on-line method called the practical filtering was proposed in [59] to estimate the parameters based on fixed-lag approximations.

One common assumption in the aforementioned methods is the structures or part of parameters of the dynamic and measurement models are known, which often cannot be satisfied in real-world applications. To alleviate this limitation, several methods resort to combining particle filtering methods with machine learning tools such as neural networks and gradient descent. We refer to these methods as differentiable particle filters [39]–[44], [62], [63].

For dynamic models in differentiable particle filters, it was proposed in [40], [41] to parametrise dynamic models using

fully-connected neural networks with previous states and given actions as inputs. In [42], [43], [63], recurrent neural networks such as long short-term memory (LSTM) networks and gated recurrent unit (GRU) networks were applied in differentiable particle filters to model the transition of latent states. Dynamic models with known functional forms are considered in [44], while the covariance matrices for dynamic noise variables need to be learned.

For measurement models in differentiable particle filters, in robot localisation tasks reported in [40], [41], [63], the conditional likelihood of observations given states are estimated by neural networks with observations and particles as inputs. The conditional likelihood function in [42]–[44] is defined as probability density functions (PDFs) of known distributions with parameters determined by state features.

In several trivially simple cases, hand-crafted proposal distributions have shown to be effective [46], [47]. However, most existing differentiable particle filters are built with vanilla neural networks, while in general, it is not feasible to compute the density of vanilla neural networks' output. There is a lack of more general mechanisms for constructing proposal distributions in these differentiable particle filters.

A key ingredient to achieving fully differentiable particle filters is a differentiable resampling scheme [62]. Several approaches have been developed towards this direction [41]–[43], [45], [62]. One class of differentiable resampling schemes designs the particle weights after resampling as a differentiable function of particle weights before resampling such that the gradients backpropagated through resampling steps are non-zero [41], [62]. A truly differentiable resampling scheme was proposed in [42], where the deterministic and differentiable resampling output is obtained by solving an entropy-regularised optimal transport problem with the Sinkhorn algorithm [64]–[66]. It was shown that the resampling scheme proposed in [42] leads to biased but asymptotically consistent estimates of the log-likelihood. A particle transformer was introduced in [45] based on a set transformer architecture [67], [68], which needs to be trained from collected data beforehand and therefore can hardly be adapted to new tasks.

Loss functions that are often used in training differentiable particle filters can be grouped into two main classes. The first class is the likelihood-based loss functions [46]–[48]. In [46]–[48], an evidence lower bound (ELBO) of observation log-likelihood was derived within a general particle filtering framework and maximised to learn system models and proposal distributions [42], [46]. The other type of loss functions involves task-specific objectives, e.g. root mean square error (RMSE) between estimates of states and ground-truth states [40]–[42], [63], among others [12], [63], [69], [70]. It was reported in [63] that combining task-specific loss functions with log-likelihood objectives gives the best empirical performance in numerical simulations.

## II. PROBLEM STATEMENT

We consider filtering problems in state-space models (SSMs). State-space models refer to a class of sequential models that consist of two discrete-time variables, the latent

state variable  $(x_t)_{t \geq 0}$  defined on  $\mathcal{X} \subseteq \mathbb{R}^{d_x}$ , and the observed measurement variable  $(y_t)_{t \geq 0}$  defined on  $\mathcal{Y} \subseteq \mathbb{R}^{d_y}$  [71]. The latent state  $(x_t)_{t \geq 0}$  is characterised by a Markov process with an initial distribution  $\pi(x_0)$  and a transition kernel  $p(x_t|x_{t-1}; \theta)$  for  $t \geq 1$ . The observation  $y_t$  is conditionally independent given the current latent state  $x_t$ :

$$x_0 \sim \pi(x_0; \theta), \quad (1)$$

$$x_t|x_{t-1} \sim p(x_t|x_{t-1}; \theta) \text{ for } t \geq 1, \quad (2)$$

$$y_t|x_t \sim p(y_t|x_t; \theta) \text{ for } t \geq 0, \quad (3)$$

where  $\theta \in \Theta$  is the parameter set of interest. Denoted by  $x_{0:t} := \{x_0, \dots, x_t\}$  and  $y_{0:t} := \{y_0, \dots, y_t\}$  the sequences of latent states and observations up to time step  $t$  respectively. In this work, our goal is to jointly estimate the joint posterior distribution  $p(x_{0:t}|y_{0:t}; \theta)$  or the marginal posterior distribution  $p(x_t|y_{0:t}; \theta)$  and the parameter set  $\theta$ .

## III. PRELIMINARIES

### A. Particle Filtering

Except for a limited class of state-space models such as linear Gaussian models [72], analytical solutions for the posterior distribution  $p(x_{0:t}|y_{0:t}; \theta)$  are unavailable since they involve complex high-dimensional integrations over  $\mathcal{X}^{t+1}$ . Particle filters are an alternative solution to the above problem. In particular, particle filters approximate intractable joint posteriors with empirical distributions consisting of sets of weighted samples  $\{\mathbf{w}_t^i, x_{0:t}^i\}_{i \in [N]}$ :

$$p(x_{0:t}|y_{0:t}; \theta) \approx \sum_{i=1}^N \mathbf{w}_t^i \delta_{x_{0:t}^i}(x_{0:t}), \quad (4)$$

where  $[N] := \{1, \dots, N\}$ ,  $N$  is the number of particles,  $\delta_{x_{0:t}^i}(\cdot)$  denotes the Dirac delta function located in  $x_{0:t}^i$ , and  $\mathbf{w}_t^i \geq 0$  with  $\sum_{i=1}^N \mathbf{w}_t^i = 1$  is the normalised importance weight of the  $i$ -th particle at the  $t$ -th time step. Particles with higher importance weights are believed to be closer to the true state than those with lower importance weights. The particles  $\{x_{0:t}^i\}_{i \in [N]}$  are sampled from proposal distributions  $q(x_0|y_0; \phi)$  when  $t = 0$  and  $q(x_t|y_t, x_{t-1}; \phi)$  for  $t \geq 1$ . Denote by  $w_t^i$  unnormalised importance weights of particles, importance weights of particles are updated recursively through:

$$w_t^i = w_{t-1}^i \frac{p(y_t|x_t^i; \theta)p(x_t^i|x_{t-1}^i; \theta)}{q(x_t^i|y_t, x_{t-1}^i; \phi)}, \quad (5)$$

with  $w_0^i = \frac{p(y_0|x_0^i; \theta)\pi(x_0^i; \theta)}{q(x_0^i|y_0; \phi)}$  and normalised as  $\mathbf{w}_t^i = \frac{w_t^i}{\sum_{j=1}^N w_t^j}$ . Particle resampling is triggered when a predefined condition is satisfied [73], [74].

### B. Differentiable particle filters

In differentiable particle filters, both the evolution of latent state  $x_t$  and the relationship between the observation  $y_t$  and the latent state  $x_t$  are modelled by neural networks. Particularly, differentiable particle filters describe the transition of the state  $x_t$  using a parametrised function  $g_\theta(\cdot) : \mathcal{X} \times \mathbb{R}^{d_s} \rightarrow \mathcal{X}$ :

$$x_t = g_\theta(x_{t-1}, \varsigma_t) \sim p(x_t|x_{t-1}; \theta), \quad (6)$$

where  $\varsigma_t \in \mathbb{R}^{d_\varsigma}$  is the noise variable used to simulate the dynamic noise, and  $g_\theta(\cdot)$  is differentiable w.r.t.  $x_t$  and  $\varsigma_t$ . For measurement models, one commonly adopted construction is through a parametrised function  $l_\theta(\cdot) : \mathcal{Y} \times \mathcal{X} \rightarrow \mathbb{R}$ :

$$p(y_t|x_t; \theta) \propto l_\theta(y_t, x_t), \quad (7)$$

$l_\theta(\cdot)$  measures compatibilities between  $y_t$  and  $x_t$  and needs to be differentiable w.r.t. both  $y_t$  and  $x_t$ . Similarly, the proposal distribution can also be constructed through a parametrised function  $f_\phi(\cdot) : \mathcal{X} \times \mathcal{Y} \times \mathbb{R}^{d_v} \rightarrow \mathcal{X}$ :

$$x_t = f_\phi(x_{t-1}, y_t, v_t) \sim q(x_t|x_{t-1}, y_t; \phi), \quad (8)$$

where  $v_t \in \mathbb{R}^{d_v}$  refers to the sampling noise.

While it has been widely documented that the resampling step is non-differentiable [41], [62], several approaches have been developed to solve this problem [41]–[43], [45], [62]. With the differentiable components discussed above, differentiable particle filters are optimised by minimising a loss function through gradient descent.

### C. Normalising flows

Consider a  $D$ -dimensional variable  $z \sim p_Z(z)$ , where  $p_Z(\cdot)$  is a known simple distribution, e.g. Gaussian, defined on  $\mathcal{Z} \subseteq \mathbb{R}^D$ . We define a variable  $s$  on  $\mathcal{S} \subseteq \mathbb{R}^D$  through a transformation  $s = \mathcal{T}_\theta(z)$ ,  $\mathcal{T}_\theta(\cdot) : \mathcal{Z} \rightarrow \mathcal{S}$ , where  $\theta$  is the parameter of the transformation. The transformation  $\mathcal{T}_\theta(\cdot)$  is called a normalising flow if it is invertible w.r.t.  $z$  and differentiable w.r.t.  $\theta$  and  $z$  [75], [76]. Under some mild assumptions,  $s = \mathcal{T}_\theta(z)$  can represent arbitrarily complex distributions, even if the distribution of  $z$  is as simple as a standard Gaussian [76].

Recent developments in normalising flows focus on constructing invertible transformations with neural networks [77]–[82]. Compared with vanilla neural networks which cannot produce valid probability densities, the density of normalising flows' output  $s = \mathcal{T}_\theta(z)$  can be obtained by applying the change of variable formula. Since the composition of a series of invertible and differentiable transformations is still invertible and differentiable, we can stack  $K$  simple invertible transformations  $\{\mathcal{T}_{\theta_k}(\cdot)\}_{k=1}^K$  together and yield a more expressive normalising flows  $s = \mathcal{T}_{\theta_K} \circ \mathcal{T}_{\theta_{K-1}} \circ \dots \circ \mathcal{T}_{\theta_1}(z)$ . Correspondingly, the density of  $s$  can be computed by successively applying the change of variable formula.

One simple example of normalising flows is the planar flow [80]. Denote by  $z \in \mathbb{R}^D$  the input of planar flows, a planar flow transforms  $z$  as follows:

$$\mathcal{T}_\theta(z) = z + vh(w^\top z + b), \quad (9)$$

where  $\mathcal{T}_\theta(\cdot)$  is parametrised by  $\theta := \{w \in \mathbb{R}^D, v \in \mathbb{R}^D, b \in \mathbb{R}\}$ , and  $h(\cdot) : \mathbb{R} \rightarrow \mathbb{R}$  is a smooth non-linear function. It has been proved in [80] that Eq. (9) is invertible when some mild conditions on  $w$ ,  $u$ , and  $h(\cdot)$  are satisfied. The Jacobian determinant of planar flow can be computed in  $\mathcal{O}(D)$  time.

Another variant of normalising flows, the Real-NVP model [77], constructs invertible transformations through coupling layers. In standard coupling layers the input  $z$  is split into two parts  $z = [z_1, z_2]$ , where  $z_1 = z_{1:d}$  refers to the first

$d$  dimensions of  $z$ , and  $z_2 = z_{d+1:D}$  refers to the last  $D - d$  dimensions of  $z$ . The partition is uniquely determined by an index  $d < D$ , and the output  $s \in \mathbb{R}^D$  of the coupling layer is given by:

$$\begin{matrix} s \\ 1:d \end{matrix} = \begin{matrix} z \\ 1:d \end{matrix}, \quad (10)$$

$$\begin{matrix} s \\ d+1:D \end{matrix} = \begin{matrix} z \\ d+1:D \end{matrix} \odot e^{\gamma_\theta(\begin{matrix} z \\ 1:d \end{matrix})} + \eta_\theta(\begin{matrix} z \\ 1:d \end{matrix}), \quad (11)$$

where  $\gamma_\theta(\cdot) : \mathbb{R}^d \rightarrow \mathbb{R}^{D-d}$  and  $\eta_\theta(\cdot) : \mathbb{R}^d \rightarrow \mathbb{R}^{D-d}$  stand for the scale function and the translation function, respectively, and  $\odot$  refers to element-wise products. With the special structure defined by Eq. (10), coupling layers are invertible by design, and Jacobian matrices of coupling layers are lower or upper triangular matrices, such that the Jacobian determinants can be efficiently computed. In addition to coupling layers, more tricks to build expressive invertible transformations such as multi-scale structure, masked convolution, and batch normalisation can be found in [77].

To model the conditional probability density of  $s$  conditioned on  $u \in \mathbb{R}^{d_u}$ , i.e.  $p(s|u; \phi)$ , one can use another type of normalising flows, called conditional normalising flow [83], [84]. Both planar flows and Real-NVP models have their conditional counterparts. Given a condition  $u \in \mathbb{R}^{d_u}$ , a planar flow can be made conditional with the following modification:

$$\mathcal{F}_\phi(z; u) = z + vh(w^\top z + b \odot s(u)), \quad (12)$$

where  $s(\cdot) : \mathbb{R}^{d_u} \rightarrow \mathbb{R}^D$  can be any linear or non-linear functions and does not impair the invertibility of the flow. Conditional Real-NVP models were proposed in [83] by replacing standard coupling layers with conditional coupling layers. Compared to standard coupling layers, the scale and translation functions in conditional coupling layers are functions of concatenations of the base variable  $z_1 = z_{1:d}$  and a given condition  $u \in \mathbb{R}^{d_u}$ , i.e. the input of the translation and scale functions now becomes  $[\begin{matrix} z \\ 1:d \end{matrix}, u]$ . Specifically, a conditional coupling layer can be formulated as:

$$\begin{matrix} s \\ 1:d \end{matrix} = \begin{matrix} z \\ 1:d \end{matrix}, \quad (13)$$

$$\begin{matrix} s \\ d+1:D \end{matrix} = \begin{matrix} z \\ d+1:D \end{matrix} \odot e^{\tilde{\gamma}_\phi(\begin{matrix} z \\ 1:d \end{matrix}, u)} + \tilde{\eta}_\phi(\begin{matrix} z \\ 1:d \end{matrix}, u), \quad (14)$$

where  $\tilde{\gamma}_\phi(\cdot) : \mathbb{R}^{d+d_u} \rightarrow \mathbb{R}^{D-d}$  and  $\tilde{\eta}_\phi(\cdot) : \mathbb{R}^{d+d_u} \rightarrow \mathbb{R}^{D-d}$  stand for the conditional scale function and the conditional translation function, respectively.

## IV. NORMALISING FLOW-BASED DIFFERENTIABLE PARTICLE FILTERS

In this section, we present details of the proposed normalising flow-based differentiable particle filter (NF-DPF), including its dynamic model, measurement model, and proposal distribution. Specifically, we first show that normalising flows can provide a flexible mechanism for learning complex dynamics of latent states. In addition, the construction of proposal distributions with tractable proposal densities can also be achieved using conditional normalising flows. Lastly, we elaborate on

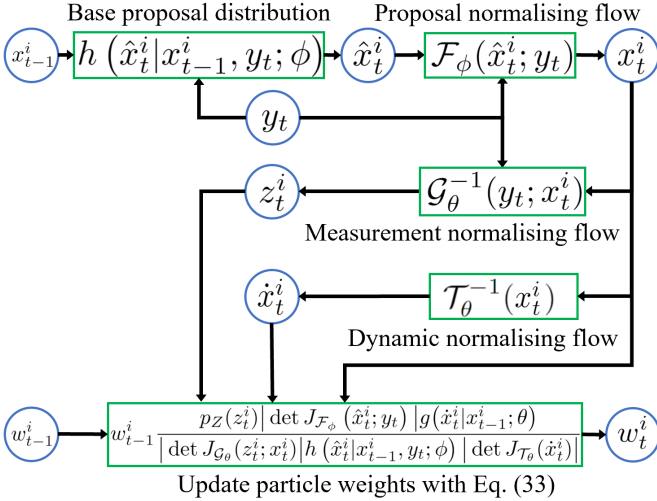


Fig. 1: A diagram that shows the overall structure of the proposed NF-DPF, illustrating how to generate new particles and update particle weights in NF-DPFs. Blue circles refer to random variables. Green rectangles refer to operations such as drawing samples or evaluating certain functions.

how to construct measurement models with valid probability densities using conditional normalising flows. An illustration of the structure of the proposed NF-DPF is presented in Fig. 1.

### A. Dynamic models with normalising flows

We first show how to use normalising flows to construct flexible dynamic models. Here we consider a base distribution  $g(\cdot|x_{t-1}; \theta)$ , e.g. Gaussian distribution, from which we can draw samples and obtain tractable probability density, and a normalising flow  $\mathcal{T}_\theta(\cdot) : \mathcal{X} \rightarrow \mathcal{X}$  parametrised by  $\theta$ . To draw samples from the proposed dynamic model, a set of particles  $\{\hat{x}_t^i\}_{i=1}^N$  are first drawn from  $g(\cdot|x_{t-1}; \theta)$ . Thereafter,  $\{\hat{x}_t^i\}_{i=1}^N$  are further transformed by the normalising flow  $\mathcal{T}_\theta(\cdot)$  and considered as samples from  $p(x_t|x_{t-1}; \theta)$ :

$$\hat{x}_t^i \sim g(\hat{x}_t^i|x_{t-1}; \theta), \quad (15)$$

$$x_t^i = \mathcal{T}_\theta(\hat{x}_t^i) \sim p(x_t|x_{t-1}; \theta). \quad (16)$$

By applying the change of variable formula, the probability density function of the proposed dynamic model can be formulated as:

$$p(x_t|x_{t-1}; \theta) = g(\hat{x}_t^i|x_{t-1}; \theta) \left| \det J_{\mathcal{T}_\theta}(\hat{x}_t^i) \right|^{-1}, \quad (17)$$

$$\hat{x}_t^i = \mathcal{T}_\theta^{-1}(x_t^i) \sim g(\hat{x}_t^i|x_{t-1}; \theta), \quad (18)$$

where  $\det J_{\mathcal{T}_\theta}(\hat{x}_t^i)$  is the Jacobian determinant of  $\mathcal{T}_\theta(\cdot)$  evaluated at  $\hat{x}_t^i = \mathcal{T}_\theta^{-1}(x_t^i)$ .

### B. Proposal distributions with conditional normalising flows

We propose to incorporate information from observations to construct proposal distributions by using conditional normalising flows. We use  $\mathcal{F}_\phi(\cdot) : \mathcal{X} \times \mathcal{Y} \rightarrow \mathcal{X}$  to denote a conditional normalising flow defined on  $\mathcal{X} \times \mathcal{Y}$ , where  $\mathcal{X}$  and  $\mathcal{Y}$  are the range of state  $x_t$  and observation  $y_t$ , respectively. In the proposed method, particles sampled from the proposal

distributions are obtained by transforming samples from a base proposal distribution  $h(\cdot|x_{t-1}, y_t; \phi)$ ,  $t \geq 1$ , and  $h_0(\cdot|y_0; \phi)$ ,  $t = 0$ , with the conditional normalising flow  $\mathcal{F}_\phi(\cdot)$ :

$$\hat{x}_0^i \sim h_0(\hat{x}_0^i|y_0; \phi), \quad (19)$$

$$\hat{x}_t^i \sim h(\hat{x}_t^i|x_{t-1}, y_t; \phi), \quad (20)$$

$$x_0^i = \mathcal{F}_\phi(\hat{x}_0^i; y_0) \sim q(x_0|y_0; \phi), \quad (21)$$

$$x_t^i = \mathcal{F}_\phi(\hat{x}_t^i; y_t) \sim q(x_t|x_{t-1}, y_t; \phi). \quad (22)$$

The base proposal distribution  $h(\cdot|x_{t-1}, y_t; \phi)$  is a distribution with a tractable probability density which we can draw samples from, e.g. a Gaussian distribution. The conditional normalising flow  $\mathcal{F}_\phi(\cdot)$  is an invertible function of particles  $\hat{x}_t^i$  given the observation  $y_t$ . Since the information from observations is taken into account, the conditional normalising flow  $\mathcal{F}_\phi(\cdot)$  provides the capability to migrate particles to regions that are closer to the true posterior distributions.

The proposal density can be obtained by applying the change of variable formula:

$$q(x_t|x_{t-1}, y_t; \phi) = h(\hat{x}_t^i|x_{t-1}, y_t; \phi) \left| \det J_{\mathcal{F}_\phi}(\hat{x}_t^i; y_t) \right|^{-1}, \quad (23)$$

$$\hat{x}_t^i = \mathcal{F}_\phi^{-1}(x_t^i; y_t) \sim h(\hat{x}_t^i|x_{t-1}, y_t; \phi), \quad (24)$$

where  $\det J_{\mathcal{F}_\phi}(\hat{x}_t^i; y_t)$  refers to the determinant of the Jacobian matrix  $J_{\mathcal{F}_\phi}(\hat{x}_t^i; y_t) = \frac{\partial \mathcal{F}_\phi(\hat{x}_t^i; y_t)}{\partial \hat{x}_t^i}$  evaluated at  $\hat{x}_t^i$ .

### C. Conditional normalising flow measurement models

Given an observation  $y_t$  and a state value  $x_t$ , we model the relationship between  $y_t$  and  $x_t$  through a conditional normalising flow  $\mathcal{G}_\theta(\cdot) : \mathbb{R}^{d_Y} \times \mathcal{X} \rightarrow \mathcal{Y}$ :

$$y_t = \mathcal{G}_\theta(z_t; x_t), \quad (25)$$

where  $d_Y$  is the dimension of the observation  $y_t$ ,  $z_t = \mathcal{G}_\theta^{-1}(y_t; x_t)$  is the base variable which follows a user-specified independent marginal distribution  $p_Z(z_t)$  defined on  $\mathbb{R}^{d_Y}$ , e.g. an isotropic Gaussian, and the state  $x_t$  is the condition variable. Note that the invertible transformation  $\mathcal{G}_\theta(\cdot)$  used here is a new construction of conditional normalising flow that is different from  $\mathcal{F}_\phi(\cdot)$ , as they are used to model different conditional probabilities.

With the conditional generative process of  $y_t$  defined by Eq. (25), we can evaluate the likelihood of the observation  $y_t$  given  $x_t$  through:

$$z_t = \mathcal{G}_\theta^{-1}(y_t; x_t), \quad (26)$$

$$p(y_t|x_t; \theta) = p_Z(z_t) \left| \det J_{\mathcal{G}_\theta}(z_t; x_t) \right|^{-1}. \quad (27)$$

In scenarios where observations are high-dimensional such as images, evaluating  $p(y_t|x_t; \theta)$  with Eq. (27) using raw observations  $y_t$  can be computationally expensive. As an alternative solution, we propose to map the observation  $y_t$  to a lower-dimensional space via  $e_t = E_\theta(y_t) \in \mathbb{R}^{d_e}$ , where  $E_\theta$  is a parametrised encoder function  $E_\theta(\cdot) : \mathbb{R}^{d_Y} \rightarrow \mathbb{R}^{d_e}$ . To ensure that the feature  $e_t$  maintains key features contained in  $y_t$ , we introduce a decoder  $D_\theta(\cdot) : \mathbb{R}^{d_e} \rightarrow \mathbb{R}^{d_Y}$  to reconstruct

$y_t$ , and include the following autoencoder (AE) loss into the training objective:

$$\mathcal{L}_{\text{AE}}(\theta) = \frac{1}{T} \sum_{t=0}^T \|D_\theta(E_\theta(y_t)) - y_t\|_2^2, \quad (28)$$

where  $T$  is the trajectory length. We then assume that the conditional probability density  $p(e_t|x_t; \theta)$  of observation features given state is an approximation of the actual measurement likelihood  $p(y_t|x_t; \theta)$  [42]:

$$e_t = E_\theta(y_t), \quad (29)$$

$$z_t = \mathcal{G}_\theta^{-1}(e_t; x_t), \quad (30)$$

$$p(y_t|x_t; \theta) \approx p(e_t|x_t; \theta) \quad (31)$$

$$= p_Z(z_t) \left| \det J_{\mathcal{G}_\theta}(z_t; x_t) \right|^{-1}. \quad (32)$$

#### D. Importance weights update

Combining Eqs. (17), (23), and (32), in the proposed normalising flow-based differentiable particle filters, importance weights of  $x_t^i \sim q(x_t^i|x_{t-1}^i, y_t; \phi)$  for  $t \geq 1$  are updated as follows:

$$\begin{aligned} w_t^i &\propto w_{t-1}^i \frac{p(y_t|x_t^i; \theta)p(x_t^i|x_{t-1}^i; \theta)}{q(x_t^i|x_{t-1}^i, y_t; \phi)} \\ &= w_{t-1}^i \frac{p_Z(z_t^i) \left| \det J_{\mathcal{F}_\phi}(\hat{x}_t^i; y_t) \right| g(\hat{x}_t^i|x_{t-1}^i; \theta)}{\left| \det J_{\mathcal{G}_\theta}(z_t^i; x_t^i) \right| h(\hat{x}_t^i|x_{t-1}^i, y_t; \phi) \left| \det J_{\mathcal{T}_\theta}(\hat{x}_t^i) \right|}, \end{aligned} \quad (33)$$

where  $z_t^i$  is computed by either Eq. (30) or Eq. (26),  $\hat{x}_t^i = \mathcal{F}_\phi^{-1}(x_t; y_t)$ ,  $\hat{x}_t^i = \mathcal{T}_\theta^{-1}(x_t^i)$ , and  $w_0^i$  is obtained by:

$$w_0^i = \frac{p_Z(z_0^i) \left| \det J_{\mathcal{F}_\phi}(\hat{x}_0^i; y_0) \right| \pi(x_0^i; \theta)}{h_0(\hat{x}_0^i|y_0; \phi) \left| \det J_{\mathcal{G}_\theta}(z_0^i; x_0^i) \right|}. \quad (35)$$

We provide in Algorithm 1 a detailed description of the proposed normalising flow-based differentiable particle filters (NF-DPFs), where we use the entropy-regularised optimal transport resampler  $\mathcal{R}_\epsilon(\{x_t^i\}_{i \in [N]}, \{\mathbf{w}_t^i\}_{i \in [N]}) : \mathbb{R}^{N \times d_x} \times \mathbb{R}^N \rightarrow \mathbb{R}^{N \times d_x}$  in resampling steps [42], and denote the entropy regularisation coefficient by  $\epsilon$ , the base distribution  $p_Z(\cdot)$  is set to be a standard Gaussian distribution.

## V. THEORETICAL ANALYSIS

In this section, we establish convergence results for particle approximations in normalising flow-based differentiable particle filters. We assume resampling is performed at each time step using the entropy-regularised optimal transport resampler [42]. We use the notations below for the following contents:

$$\alpha^{(t)} := p(x_t|y_{0:t-1}; \theta), \quad \alpha_N^{(t)}(\psi) := \frac{1}{N} \sum_{i=1}^N \psi(x_t^i), \quad (36)$$

$$\beta^{(t)} := p(x_t|y_{0:t}; \theta), \quad \beta_N^{(t)}(\psi) := \sum_{i=1}^N \mathbf{w}_t^i \psi(x_t^i), \quad (37)$$

$$\omega^{(t)}(x_t) = p(y_t|x_t; \theta), \quad (38)$$

## Algorithm 1 Normalising flow-based differentiable particle filters

### 1: Notations:

$T$	Trajectory length	$x_{0:T}$	Latent states
$y_{0:T}$	Observations	$\pi(\cdot; \theta)$	Initial distribution of latent states
$g(\cdot)$	Base dynamic model	$\mathcal{T}_\theta(\cdot)$	Dynamic model normalising flow
$\mathcal{F}_\phi(\cdot)$	Proposal normalising flow	$\mathcal{G}_\theta(\cdot)$	Measurement normalising flow
$N$	Number of particles	$\text{ESS}_{\min}$	Resampling threshold
$\xi$	Learning rate	$\mathcal{L}(\theta, \phi)$	Overall loss function
$E_\theta(\cdot)$	Observation encoder	$\mathcal{R}_\epsilon(\cdot)$	Regularised OT resampler [42]
$\epsilon$	Regularisation coefficient	$p_Z(\cdot)$	Standard Gaussian distribution

### 2: Initialisation: Randomly initialise $\theta$ and $\phi$ ;

Sample  $\hat{x}_0^i \stackrel{\text{i.i.d.}}{\sim} h_0(\hat{x}_0|y_0; \phi)$ ,  $\forall i \in [N] := \{1, \dots, N\}$  (Eq. (19));

### 3: Generate proposed particles (Eq. (21)):

$x_0^i = \mathcal{F}_\phi(\hat{x}_0^i; y_0) \sim q(x_0|y_0; \phi)$ ,  $\forall i \in [N]$ ;

### 4: [optional] Encode observation (Eq. (29)): $y_0 := E_\theta(y_0)$ ;

### 5: Compute the base variable (Eq. (30)):

$z_0^i = \mathcal{G}_\theta^{-1}(y_0; x_0^i)$ ,  $\forall i \in [N]$ ;

### 6: Compute weights $w_0^i$ using Eq. (35), $\forall i \in [N]$ ;

### 7: [optional] $\hat{p}(y_0; \theta) = \sum_{i=1}^N w_0^i / N$ ;

### 8: for $t = 1$ to $T$ do

#### 9: Normalise weights $\mathbf{w}_{t-1}^i \propto w_{t-1}^i$ , $\sum_{i=1}^N \mathbf{w}_{t-1}^i = 1$ ;

#### 10: Compute the effective sample size:

$$\text{ESS}_{t-1}(\{\mathbf{w}_{t-1}^i\}_{i \in [N]}) = \frac{1}{\sum_{i=1}^N (\mathbf{w}_{t-1}^i)^2};$$

#### 11: if $\text{ESS}_{t-1}(\{\mathbf{w}_{t-1}^i\}_{i \in [N]}) < \text{ESS}_{\min}$ then

$\{\tilde{x}_{t-1}^i\}_{i=1}^N \leftarrow \mathcal{R}_\epsilon(\{\mathbf{w}_{t-1}^i\}_{i \in [N]}, \{\mathbf{w}_{t-1}^i\}_{i \in [N]})$ ;

#### 12: $\hat{x}_{t-1}^i \leftarrow \tilde{x}_{t-1}^i$ , $\forall i \in [N]$ ;

#### 13: else

$\hat{x}_{t-1}^i \leftarrow x_{t-1}^i$ ,  $\forall i \in [N]$ ;

#### 14: end if

$x_{t-1}^i \leftarrow \hat{x}_{t-1}^i$ ;

#### 15: Sample $\hat{x}_t^i \stackrel{\text{i.i.d.}}{\sim} h(\hat{x}_t|x_{t-1}, y_t; \phi)$ , $\forall i \in [N]$ (Eq. (19));

#### 16: Generate proposed particles (Eq. (22)):

$x_t^i = \mathcal{F}_\phi(\hat{x}_t^i; y_t) \sim q(x_t|x_{t-1}, y_t; \phi)$ ,  $\forall i \in [N]$ ;

#### 17: [Optional] Encode observation: $y_t := E_\theta(y_t)$ ;

#### 18: Compute the base variable (Eq. (30)):

$z_t^i = \mathcal{G}_\theta^{-1}(y_t; x_t^i)$ ,  $\forall i \in [N]$ ;

#### 19: Update weights using Eq. (34):

$$w_t^i = w_{t-1}^i \frac{p(y_t|x_t^i; \theta)p(x_t^i|x_{t-1}^i; \theta)}{q(x_t^i|x_{t-1}^i, y_t; \phi)}, \quad \forall i \in [N];$$

#### 20: [optional] $\hat{p}(y_t|y_{0:t-1}; \theta) = \sum_{i=1}^N w_t^i / \sum_{i=1}^N w_{t-1}^i$ ,

$$\hat{p}(y_{0:t}; \theta) = \hat{p}(y_t|y_{0:t-1}; \theta) \hat{p}(y_{0:t-1}; \theta);$$

#### 21: end for

#### 22: Compute the overall loss function $\mathcal{L}(\theta, \phi)$ ;

#### 23: Update $\theta$ and $\phi$ through gradient descent:

$$\theta \leftarrow \theta - \xi \nabla_\theta \mathcal{L}(\theta, \phi), \quad \phi \leftarrow \phi - \xi \nabla_\phi \mathcal{L}(\theta, \phi).$$

with  $\alpha^{(0)} := \pi(x_0; \theta)$ ,  $\psi(\cdot) : \mathcal{X} \rightarrow \mathbb{R}$  is a function defined on  $\mathcal{X}$ ,  $\alpha_N^{(t)}$  is an approximation of the predictive distribution  $\alpha^t$  with  $N$  uniformly weighted particles, and  $\beta_N^{(t)}$  is an approximation of the posterior distribution  $\beta^{(t)}$  with  $N$  particles weighted by  $\mathbf{w}_t^i$ . For a measure  $\alpha$  defined on  $\mathcal{X}$  we use  $\alpha(\psi) = \int_{\mathcal{X}} \psi(x) \alpha(dx)$  to denote the expectation of  $\psi(\cdot)$  w.r.t.  $\alpha$ . For the sake of simplicity, we restrict ourselves to the bootstrap particle filtering framework, i.e. particles

$x_t^i$  are sampled from  $p(x_t|x_{t-1};\theta)$ . However, our proof can be modified to adapt to particle filters employing proposal distributions that are distinct from their dynamic models by taking into account the estimation error caused by sampling from  $q(x_t|x_{t-1}, y_t; \phi)$  instead of  $p(x_t|x_{t-1};\theta)$ .

To prove the consistency of particle approximations provided by NF-DPFs, we introduce the following assumptions:

**Assumption V.1.**  $\mathcal{X}$  is a compact subset of  $\mathbb{R}^{d_x}$  with diameter  $\mathfrak{d} := \sup_{x, x' \in \mathcal{X}} \|x - x'\|_2$ , where  $\|\cdot\|_2$  denotes the Euclidean distance.

**Assumption V.2.** For  $\forall t \geq 0$ , there exists a unique optimal transport plan between  $\alpha^t$  and  $\beta^t$  featured by a deterministic transport map  $\mathbf{T}_t(\cdot) : \mathcal{X} \rightarrow \mathcal{X}$ , and the transport map  $\mathbf{T}_t(\cdot)$  is  $\lambda$ -Lipschitz for  $\forall t \geq 0$  with  $\lambda > 0$ .

**Assumption V.3.** Denote by  $f(\cdot)$  the transition kernel  $p(x_t|x_{t-1};\theta)$  of NF-DPFs defined in Eq. (17), there exists an  $\eta \in \mathbb{R}$  such that for any two probability measures  $\mu, \rho$  on  $\mathcal{X}$  and any bounded  $k$ -Lipschitz function  $\psi(\cdot) : \mathcal{X} \rightarrow \mathbb{R}$ ,

$$|\mu f(\psi) - \rho f(\psi)| \leq \eta |\mu(\psi) - \rho(\psi)|.$$

**Assumption V.4.** There exists a  $\zeta \in \mathbb{R}$  such that for any probability measure  $\mu$  on  $\mathcal{X}$  and its empirical approximation  $\mu_N$ , for weighted probability measures  $\mu_{\omega_t} = \omega_t \mu / \mu(\omega_t)$  and  $\mu_{N, \omega_t} = \omega_t \mu_N / \mu_N(\omega_t)$ , we have

$$\mathcal{W}_2(\mu_{N, \omega_t}, \mu_{\omega_t}) \leq \zeta \mathcal{W}_2(\mu_N, \mu),$$

where  $\omega_t(\cdot) : \mathcal{X} \rightarrow \mathbb{R}$  is defined in Eq. (38), and  $\mathcal{W}_2(\cdot, \cdot)$  refers to the 2-Wasserstein distance [66], [85].

With the above assumptions, we provide the following proposition for the consistency of NF-DPFs:

**Proposition V.1.** For a bounded weight function  $\omega_t(x_t) = p(y_t|x_t; \theta) : \mathcal{X} \rightarrow \mathbb{R}$  and a measurable bounded  $k$ -Lipschitz function  $\psi(\cdot) : \mathcal{X} \rightarrow \mathbb{R}$ , when the regularisation coefficient in entropy-regularised optimal transport resampler  $\epsilon_N = o(1/\log N)$ , there exist constants  $c_t$  and  $c'_t$  such that for  $t \geq 0$

$$\mathbb{E} \left[ \left( \alpha_N^{(t)}(\psi) - \beta^{(t-1)} f(\psi) \right)^2 \right] \leq c_t \frac{\|\psi\|_\infty^2}{N^{1/2d_x}} \quad (39)$$

(replacing  $\beta^{(t-1)} f$  by the initial distribution  $\pi(x_0, \theta)$  at time  $t = 0$  defined in Eq. (1)) and

$$\mathbb{E} \left[ \left( \beta_N^{(t)}(\psi) - \beta^{(t)}(\psi) \right)^2 \right] \leq c'_t \frac{\|\psi\|_\infty^2}{N^{1/2d_x}}, \quad (40)$$

where  $\beta^{(t)}$  and  $\alpha_N^{(t)}$  are respectively defined by Eqs. (36) and (37), and  $f(\cdot)$  is the transition kernel defined by Eq. (2).

The proof of Proposition V.1 can be found in Appendix B. The results in Proposition V.1 show that the particle estimates given by the NF-DPF are consistent estimators if  $\epsilon_N = o(1/\log N)$ , i.e. the estimation error vanishes when  $N \rightarrow \infty$ . The error bounds we derived converge at  $\mathcal{O}_P(\frac{1}{N^{1/2d_x}})$  and are tighter than those derived in [42], which converge at  $\mathcal{O}_P(\frac{1}{N^{1/8d_x}})$ , where  $\mathcal{O}_P$  denotes the "big O in probability" notation. However, compared with traditional particle filters [86],

the error bound is loose due to the use of entropy-regularised optimal transport resampling, as we revealed in the proof. We provide background knowledge about optimal transport and related notations in Appendix A.

## VI. EXPERIMENTS

In this section, we present experimental results to compare the performance of the proposed normalising flow-based differentiable particle filters (NF-DPFs) with other DPF variants. We consider in Section VI-A a one-dimensional linear Gaussian state-space model similar to an example used in [47]. In Section VI-B we evaluate the performance of the proposed method on a multivariate linear Gaussian state-space model similar to the one used in [42] with varying dimensionalities. In Section VI-C we compare the performance of NF-DPFs with other state-of-the-art DPFs in a synthetic visual tracking task following the setup in [44], [51], [87]. The experimental results on a simulated robot localisation task from [40], [42], [88] are reported in Section VI-D. For all experiments presented in this section, the entropy-regularised optimal transport resampler [42] is applied in the resampling step. We use the Real-NVP and the conditional Real-NVP models as the default normalising flows and conditional normalising flows in the NF-DPF, except in the one-dimensional example, because Real-NVP models have to split the latent state dimension-wise.

We compare NF-DPFs with four baseline methods in our experiments, the autoencoder sequential Monte Carlo (AESMC) and the AESMC-bootstrap proposed in [47], the particle filter recurrent neural networks (PFRNNs) [63], and the particle filter networks (PFNets) [41]. The AESMC-bootstrap uses Gaussian distributions to construct its dynamic model and measurement model and new particles are generated from the learned dynamic model. The proposal distributions of the AESMC are constructed by Gaussian distributions with parameters determined by observations. The PFRNN uses recurrent neural networks with observations and latent states as inputs to generate new particles. We use PFNets to denote the method proposed in [41] and its concurrent work [40], which are bootstrap differentiable particle filters with dynamic models and measurement models built by vanilla neural networks.

### A. One-dimensional Linear Gaussian State-Space Models

1) *Experiment setup:* We first consider a one-dimensional example as in [47], for which the goal is to learn the parameters  $\theta^* := [\theta_1^*, \theta_2^*]$  and a proposal distribution  $q(x_t|x_{t-1}, y_t; \phi)$  for the following linear Gaussian state-space model:

$$x_0 \sim \mathcal{N}(0, 1), \quad (41)$$

$$x_t|x_{t-1} \sim \mathcal{N}(\theta_1^* x_{t-1}, 1) \text{ for } t \geq 1, \quad (42)$$

$$y_t|x_t \sim \mathcal{N}(\theta_2^* x_t, 0.1) \text{ for } t \geq 0. \quad (43)$$

We adopt the evidence lower bound (ELBO)  $\mathbb{E}[\log p(y_{0:T}; \theta)]$  of the log marginal likelihood as the training objective as in [46]–[48], and we approximate the ELBO through:

$$\mathbb{E}[\log p(y_{0:T}; \theta)] \approx \frac{1}{K} \sum_{k=1}^K \log \hat{p}(y_T^k; \theta), \quad (44)$$

where  $K = 10$  is the number of training sequences, and  $\log \hat{p}(y_T^k; \theta)$  is computed as in Line 23 of Alg. 1. We use a fixed learning rate of 0.002 and optimise the model for 500 iterations. At each iteration, we feed the model  $K = 10$  sequences of observations  $y_{0:T}$  generated with  $T = 50$  and  $\theta^* := [\theta_1^*, \theta_2^*] = [0.9, 0.5]$ . We also use 1000 sequences of observations as our validation set. The trained model is then tested with another 1000 sequence of observations. We set the number of particles as  $N = 100$  for training, validation, and testing stages. Since the goal in this experiment is to simultaneously learn the model parameters  $\theta := [\theta_1, \theta_2]$  (initialised as  $[0.1, 0.1]$ ) and proposal distributions  $q(x_t|x_{t-1}, y_t; \phi)$ , the state-space model to be optimised is in the same form as the true model:

$$x_0 \sim \mathcal{N}(0, 1), \quad (45)$$

$$x_t|x_{t-1} \sim \mathcal{N}(\theta_1 x_{t-1}, 1) \text{ for } t \geq 1 \quad (46)$$

$$y_t|x_t \sim \mathcal{N}(\theta_2 x_t, 0.1) \text{ for } t \geq 0, \quad (47)$$

such that we can evaluate the difference between the true model parameters and the learned model parameters.

The performance of trained models is evaluated based on four metrics:

- The  $L^2$ -norm  $\|\theta - \theta^*\|_2$  between the learned parameters  $\theta := [\theta_1, \theta_2]$  and true parameters  $\theta^* := [\theta_1^*, \theta_2^*] = [0.9, 0.5]$ ;
- The  $L^2$ -norm  $\|\bar{\chi}_T - \bar{\chi}_T^*\|_2$  between the estimated posterior means  $\bar{\chi}_T$  and the true posterior means  $\bar{\chi}_T^*$  computed by Kalman filter, where  $\bar{\chi}_T := [\bar{x}_0, \bar{x}_1, \dots, \bar{x}_T]$  and  $\bar{\chi}_T^* := [\bar{x}_0^*, \bar{x}_1^*, \dots, \bar{x}_T^*]$ ;
- The ELBO defined by Eq. (44).
- The effective sample size.

Lower  $\|\theta - \theta^*\|_2$ ,  $\|\bar{\chi}_T - \bar{\chi}_T^*\|_2$ , and higher ELBO and effective sample size indicate better performance of evaluated models.

2) *Experimental results:* We report in Fig. 2 and Table I the evaluated metrics for different methods on the validation set and the test set, respectively. We observe that the PFNet can achieve arbitrarily large ELBOs but produces poor tracking performance, so we do not report the performance of the PFNet in this experiment. The main reason for this is that the measurement model of the PFNet is constructed with vanilla neural networks, and the ELBO can be increased by simply amplifying the magnitude of the neural network's output without learning the relationship between observations and states.

For the ELBO, all methods converge to almost the same validation ELBO as demonstrated in Fig. 2c. The AESMC-bootstrap converges the fastest. We speculate that this is because it does not have proposal parameters to learn, so it can focus on learning model parameters. This is also reflected in Fig. 2a and the second column of Table I, where we can observe that all approaches produce similar parameter estimation errors after their convergence, and the AESMC-bootstrap has the highest convergence rate but exhibits slightly larger parameter estimation error than other methods. The NF-DPF converges faster than the AESMC and the PFRNN has the highest ELBO and the lowest parameter estimation error.

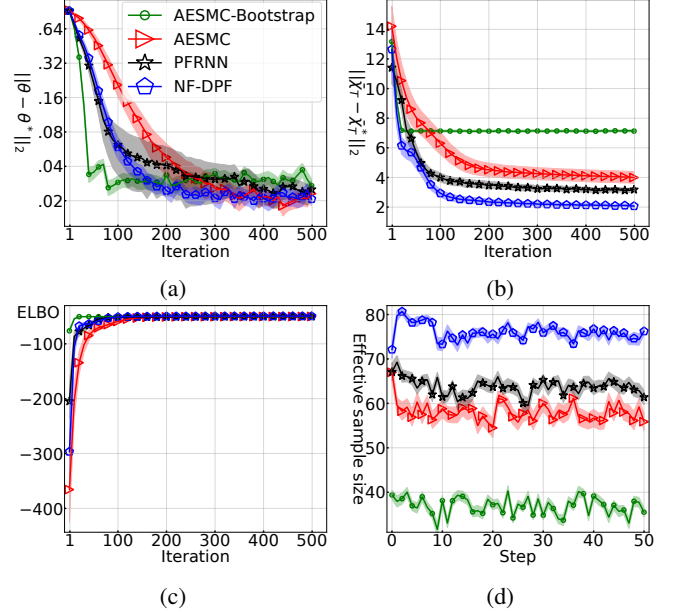


Fig. 2: Evaluation metrics of different methods evaluated on the validation set with 1000 sequences. (a)  $L^2$ -norm between the true parameter set and the estimated parameter sets. (b)  $L^2$ -norm of posterior mean error evaluated on validation set. (c) ELBO evaluated on validation set. (d) Effective sample size on validation set. Lower parameter estimation error, posterior mean error, higher effective sample size, and ELBO indicate better performance. The shaded area represents the standard deviation of the presented evaluation metrics among 50 random simulations.

We report posterior mean errors  $\|\bar{\chi}_T - \bar{\chi}_T^*\|_2$  evaluated on the validation set and the test set for different methods in Fig. 2b and Table I respectively. The AESMC-bootstrap leads to the highest estimation error as expected. The AESMC produces better results compared to the AESMC-bootstrap. The PFRNN reports the second lowest validation and test posterior mean error after the convergence. The NF-DPF outperforms all the compared baselines regarding both the convergence rate and the validation error when training has converged. The NF-DPF leads to the highest effective sample size among all the evaluated methods.

## B. Multivariate Linear Gaussian State-Space Models

1) *Experiment setup:* In this experiment, we extend the one-dimensional example in Section VI-A to higher dimensional-spaces to evaluate the performance of the NF-DPF. Following the setup in [42], we consider a similar multivariate linear Gaussian state-space model as below:

$$x_0 \sim \mathcal{N}(\mathbf{0}_{d_x}, \mathbf{I}_{d_x}), \quad (48)$$

$$x_t|x_{t-1} \sim \mathcal{N}(\theta_1^* x_{t-1}, \mathbf{I}_{d_x}) \text{ for } t \geq 1, \quad (49)$$

$$y_t|x_t \sim \mathcal{N}(\theta_2^* x_t, 0.1\mathbf{I}_{d_x}) \text{ for } t \geq 0, \quad (50)$$

where  $\mathbf{0}_{d_x}$  is a  $d_x \times d_x$  null matrix,  $\mathbf{I}_{d_x}$  is a  $d_x \times d_x$  identity matrix, the element of  $\theta_1^*$  at the intersection of its  $i$ -th row and  $j$ -th column  $\theta_1^*(i, j) = (0.42)^{|i-j|+1}$ ,  $1 \leq i, j \leq d_x$ ,



TABLE I: Evaluation metrics of different methods evaluated on the test set with 1000 sequences. Lower parameter estimation error, posterior mean error, higher effective sample size, and ELBO indicate better performance. The reported parameter estimation error, posterior mean error, and ELBO are computed with the model saved at the last iteration. The average effective sample size is the mean of effective sample sizes at each time step. The reported mean and standard deviation are computed with 50 random runs.

Method	$\ \theta - \theta^*\ _2 \downarrow$	$\ \bar{\chi}_T - \bar{\chi}_T^*\ _2 \downarrow$	Average effective sample size $\uparrow$	ELBO $\uparrow$
AESMC-Bootstrap [46]	$0.0271 \pm 0.0133$	$7.13 \pm 0.233$	$36.9 \pm 1.52$	$-50.4 \pm 1.72$
AESMC [46]	$0.0231 \pm 0.0108$	$3.99 \pm 1.316$	$58.1 \pm 14.24$	$-50.1 \pm 1.51$
PFRNN [63]	$0.0251 \pm 0.015$	$3.18 \pm 0.456$	$63.8 \pm 11.11$	$-50.1 \pm 1.94$
NF-DPF	<b><math>0.0207 \pm 0.0083</math></b>	<b><math>2.07 \pm 0.304</math></b>	<b><math>76.0 \pm 6.26</math></b>	<b><math>-49.6 \pm 1.61</math></b>

$\theta_2^*$  is a  $d_y \times d_x$  matrix with 0.5 on the diagonal for the first  $d_y$  rows and zeros elsewhere. We set  $d_x = d_y$  in this experiment. We again want to learn model parameters  $\theta^* := [\theta_1^*, \theta_2^*]$  and proposal distributions by maximising the evidence lower bound (ELBO) as in Section VI-A. We also use the same hyperparameter setting in Section VI-A, and train the compared models with 5000 sequences for 500 iterations (10 sequences for each iteration). Validation and test sets contain 1000 i.i.d sequences each. Model parameters  $\theta := [\theta_1, \theta_2]$  to be optimised are initialised as  $[0.1 \times \mathbf{I}_{d_x}, 0.1 \times \mathbf{I}_{d_x}]$ .

2) *Experimental results:* In Fig. 3 and Table II, we show the test performance of NF-DPFs, the PFRNN, and the AESMC in  $d_x$ -dimensional spaces for  $d_x \in \{2, 5, 10, 25, 50, 100\}$ . The AESMC-bootstrap particle filter is excluded in this experiment because its estimation error is too large to be compared with the other methods in the same figure. The evaluation metrics reported in Section VI-A are used in this experiment as well.

For model parameters learning, from Fig. 3a, Fig. 3c, and Table II, we found that NF-DPFs produced the highest ELBOs in 4 out of 6 setups, and all the evaluated methods achieved similar parameter estimation errors. We also observed that higher ELBOs and lower parameter estimation errors do not necessarily correspond to better posterior approximation errors as we can see from Fig. 3 and Table II. Specifically, from Fig. 3b and Table II, NF-DPFs outperform the compared baselines in terms of posterior approximation errors by consistently leading to the lowest posterior mean errors and the highest effective sample sizes for  $d_x \in \{2, 5, 10, 25, 50, 100\}$ .

### C. Disk Localisation

1) *Experiment setup:* We consider in this experiment a disk localisation task, where the goal is to locate a moving red disk based on observation images. Specifically, an observation image is a  $128 \times 128$  RGB image that contains 25 disks, including the red disk and 24 distracting disks with varying sizes and colours, and such an observation image is given at each time step. The colours of distracting disks are uniformly drawn with replacement from the set of {green, blue, cyan, purple, yellow, white}, and the radii of them are uniformly sampled with replacement from  $\{3, 4, \dots, 10\}$ . The radius of the target, i.e. the red disk, is set to be 7. The initial locations of the 25 disks are uniformly distributed over the observation image as shown in Fig. 4a.

Following the setup in [42], [50], [51], we use a combination of two loss functions as our training objective  $\mathcal{L}(\theta, \phi) :=$

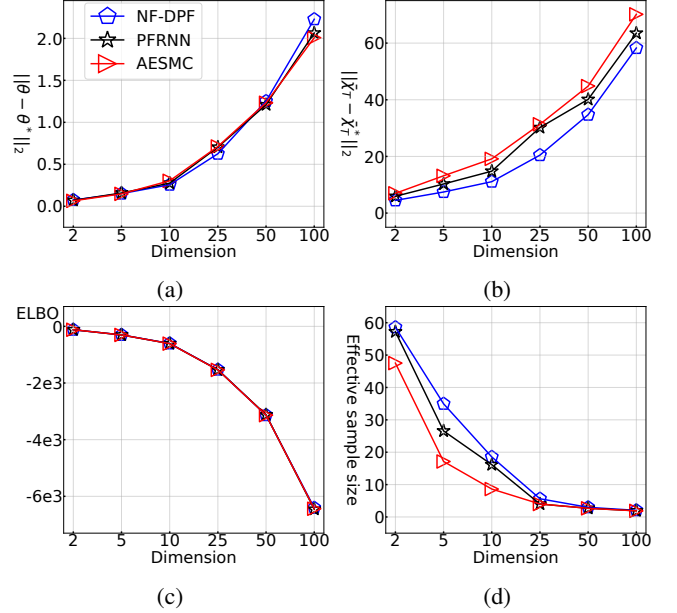


Fig. 3: Evaluation metrics of different methods evaluated on a test set with 1000 sequences. (a)  $L^2$ -norm between the true parameter set and the estimated parameter sets. (b)  $L^2$ -norm of posterior mean error evaluated on test set. (c) ELBO evaluated on test set. (d) Effective sample size on test set. Lower parameter estimation error, posterior mean error, higher effective sample size, and ELBO indicate better performance. The reported results are the mean of evaluation metrics computed over 50 random simulations.

$\mathcal{L}_{\text{RMSE}}(\theta, \phi) + \mathcal{L}_{\text{AE}}(\theta)$ , where  $\mathcal{L}_{\text{RMSE}}(\theta, \phi)$  is the root mean square error (RMSE) between the estimated location  $\bar{x}_t$  and the ground truth location  $x_t^*$  of the red disk

$$\mathcal{L}_{\text{RMSE}}(\theta, \phi) := \sqrt{\frac{1}{T} \sum_{t=0}^T \|\bar{x}_t - x_t^*\|_2^2}, \quad (51)$$

and  $\mathcal{L}_{\text{AE}}(\theta)$  is the autoencoder reconstruction loss of observation images as defined in Eq. (28). We use an Adam optimiser [89] with a learning rate of 0.001 to minimise the overall loss function  $\mathcal{L}(\theta, \phi)$ .

The dynamic system that used for generating training, validation, and test sets for this experiment follows the setup in [44]. The training set we use to optimise DPFs contains 500 trajectories, each with 50 time steps, and both the validation

TABLE II: Evaluation metrics of different methods evaluated on a test set with 1000 sequences. Lower parameter estimation error, posterior mean error, higher effective sample size, and ELBO indicate better performance. The reported parameter estimation error, posterior mean error, and ELBO are computed with the model saved at the last iteration. The average effective sample size is the mean of effective sample size at each time step. The reported mean and standard deviation is computed with 50 random runs.

Dimension	Method	$\ \theta - \theta^*\ _2 \downarrow$	$\ \bar{\chi}_T - \bar{\chi}_T^*\ _2 \downarrow$	Average effective sample size $\uparrow$	ELBO $\uparrow$
$D = 2$	AESMC [46]	<b>0.065 <math>\pm</math> 0.0226</b>	6.85 $\pm$ 1.16	47.5 $\pm$ 12.51	-119.3 $\pm$ 2.80
	PFRNN [63]	0.071 $\pm$ 0.0181	5.82 $\pm$ 1.45	57.2 $\pm$ 10.18	-119.8 $\pm$ 2.67
	NF-DPF	0.075 $\pm$ 0.0120	<b>4.48 <math>\pm</math> 0.84</b>	<b>58.6 <math>\pm</math> 6.46</b>	<b>-119.2 <math>\pm</math> 1.88</b>
$D = 5$	AESMC [46]	<b>0.148 <math>\pm</math> 0.0120</b>	13.25 $\pm$ 1.62	17.1 $\pm$ 2.83	-303.3 $\pm$ 2.64
	PFRNN [63]	0.158 $\pm$ 0.0156	10.27 $\pm$ 0.40	26.6 $\pm$ 2.60	-302.6 $\pm$ 3.19
	NF-DPF	0.151 $\pm$ 0.0105	<b>7.44 <math>\pm</math> 1.55</b>	<b>34.9 <math>\pm</math> 5.29</b>	<b>-301.6 <math>\pm</math> 3.25</b>
$D = 10$	AESMC [46]	0.304 $\pm$ 0.0214	19.17 $\pm$ 1.88	8.6 $\pm$ 1.73	-609.7 $\pm$ 6.24
	PFRNN [63]	0.275 $\pm$ 0.0148	14.89 $\pm$ 0.32	16.2 $\pm$ 1.24	-608.5 $\pm$ 7.18
	NF-DPF	<b>0.257 <math>\pm</math> 0.0116</b>	<b>11.18 <math>\pm</math> 1.28</b>	<b>18.5 <math>\pm</math> 2.37</b>	<b>-603.3 <math>\pm</math> 5.02</b>
$D = 25$	AESMC [46]	0.712 $\pm$ 0.0191	31.46 $\pm$ 2.12	4.0 $\pm$ 0.22	-1537.5 $\pm$ 12.14
	PFRNN [63]	0.704 $\pm$ 0.0312	30.21 $\pm$ 1.03	4.0 $\pm$ 0.39	-1534.2 $\pm$ 6.46
	NF-DPF	<b>0.626 <math>\pm</math> 0.0188</b>	<b>20.51 <math>\pm</math> 1.21</b>	<b>5.6 <math>\pm</math> 0.45</b>	<b>-1529.0 <math>\pm</math> 12.53</b>
$D = 50$	AESMC [46]	1.233 $\pm$ 0.0260	44.83 $\pm$ 0.92	2.7 $\pm$ 0.37	-3135.0 $\pm$ 19.56
	PFRNN [63]	<b>1.210 <math>\pm</math> 0.0222</b>	40.14 $\pm$ 0.61	2.69 $\pm$ 0.13	<b>-3121.7 <math>\pm</math> 6.39</b>
	NF-DPF	1.252 $\pm$ 0.0189	<b>34.73 <math>\pm</math> 1.81</b>	<b>3.0 <math>\pm</math> 0.11</b>	-3135.4 $\pm$ 28.53
$D = 100$	AESMC [46]	<b>2.007 <math>\pm</math> 0.0255</b>	70.16 $\pm$ 2.23	1.9 $\pm$ 0.28	<b>-6438.1 <math>\pm</math> 34.80</b>
	PFRNN [63]	2.064 $\pm$ 0.0272	63.51 $\pm$ 2.78	1.9 $\pm$ 0.47	-6454.8 $\pm$ 52.32
	NF-DPF	2.228 $\pm$ 0.0419	<b>58.27 <math>\pm</math> 1.45</b>	<b>2.0 <math>\pm</math> 0.18</b>	-6447.4 $\pm$ 80.01

and test sets are composed of 50 trajectories with the same length as training trajectories.

The performance of different DPFs is evaluated by the RMSE between estimated locations and ground truth locations of the tracking objective. We report both the test RMSE and the validation RMSE to investigate the tracking performance of different DPFs during and after training.

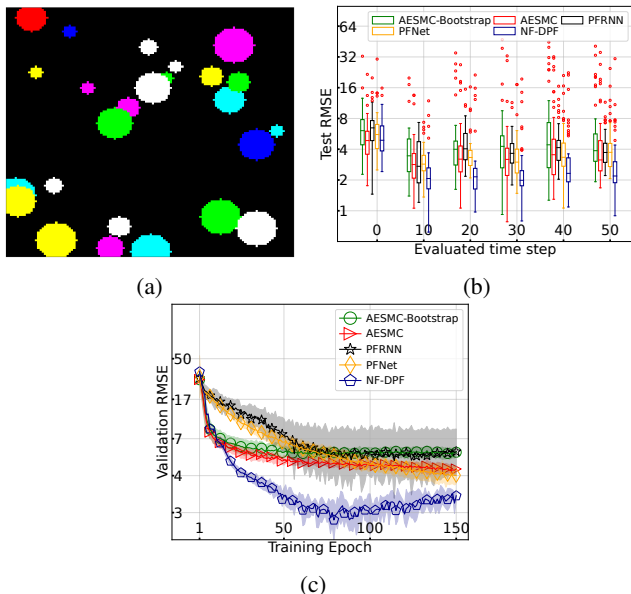


Fig. 4: (A) An example of observation images. (B) RMSE of different methods evaluated at selected time steps on test set. (C) RMSE of different differentiable particle filters on the validation set during training. Shaded areas represent the standard deviation of the presented evaluation metrics among 5 random simulations.

2) *Experimental results*: The experimental results shown in Fig. 4c are the validation RMSEs of different methods evaluated during training. It can be observed that the NF-

TABLE III: Disk tracking RMSE of different differentiable particle filters. The reported RMSE is averaged over 50 time steps for 50 trajectories in the test set, and the standard deviation is computed with 5 simulation runs with different random seeds.

Method	AESMC Bootstrap	AESMC	PFRNN	PFNet	NF-DPF
RMSE	6.35 $\pm$ 1.15	5.85 $\pm$ 1.34	6.12 $\pm$ 1.23	5.34 $\pm$ 1.27	<b>3.62<math>\pm</math>0.98</b>

DPF requires fewer training epochs to converge but in the meantime achieves better tracking performance compared with the other evaluated approaches. For all methods, we saved the best models with the lowest validation error and used them to compute the tracking error on the test set.

We report the test RMSEs of different differentiable particle filters in Table III. The experimental results in Table III again demonstrated the benefit of using (conditional) normalising flows to construct differentiable particle filters. It can be observed from Table III that among all the tested methods, the proposed NF-DPF produces the lowest mean tracking error. Fig. 4b compares tracking RMSEs from different methods on the test set. From Fig. 4b, we found that, except for the first step  $t = 1$ , the proposed NF-DPFs achieved the lowest tracking RMSE at all evaluated time steps compared with the other evaluated methods.

#### D. Robot Localisation in Maze Environments

1) *Experiment setup*: In this experiment, we evaluate the performance of NF-DPFs in three environments, namely Maze 1, Maze 2, and Maze 3, simulated in the DeepMind Lab [88] following the setup in [40], [42]. In each of the three maze environment, there exists a simulated robot moving through the maze, and its locations  $l_t = (l_t^{(1)}, l_t^{(2)})$ , orientations  $\varrho_t$ , velocity  $\Delta l_t = (\Delta l_t^{(1)}, \Delta l_t^{(2)}, \Delta \varrho_t)$ , and camera images  $y_t$  are available for model training. The collected dataset is split

into training, validation, and test sets containing 900, 100, and 100 robot trajectories, each with a length of 100 time steps, respectively. We set the learning rate to be 0.001, and use the Adam optimiser to train DPFs.

Based on image observations given by robot cameras, the goal in this task is to infer the location and the orientation of the robot at each time step, i.e. the latent state  $x_t := (l_t^{(1)}, l_t^{(2)}, \varrho_t)$ . We give an example of observation images in Fig. 5a. Particles are uniformly initialised over the maze in the first step. The dynamic model we use in DPFs is as follows:

$$x_{t+1} := \begin{bmatrix} l_{t+1}^{(1)} \\ l_{t+1}^{(2)} \\ \varrho_{t+1} \end{bmatrix} = \begin{bmatrix} l_t^{(1)} + \Delta l_t^{(1)} \cos(\varrho_t) + \Delta l_t^{(2)} \sin(\varrho_t) \\ l_t^{(2)} + \Delta l_t^{(1)} \sin(\varrho_t) - \Delta l_t^{(2)} \cos(\varrho_t) \\ \varrho_t + \Delta \varrho_t \end{bmatrix} + \varsigma_t, \quad (52)$$

where  $\varsigma_t \sim \mathcal{N}(\mathbf{0}, \Sigma^2)$  is the dynamic noise, and  $\Sigma := \text{diag}(\sigma_l, \sigma_l, \sigma_\varrho)$  with  $\sigma_l = 10$  and  $\sigma_\varrho = 0.1$ .

The loss function  $\mathcal{L}(\theta, \phi) := \mathcal{L}_{\text{RMSE}}(\theta, \phi) + \mathcal{L}_{\text{AE}}(\theta)$  used in this experiment consists of a root mean square error loss  $\mathcal{L}_{\text{RMSE}}(\theta, \phi)$  and an autoencoder loss  $\mathcal{L}_{\text{AE}}(\theta)$  as in Section VI-C. The evaluation metric we use to compare the performances of different DPFs is the RMSE error between estimated robot locations and true robot locations on validation and test sets.

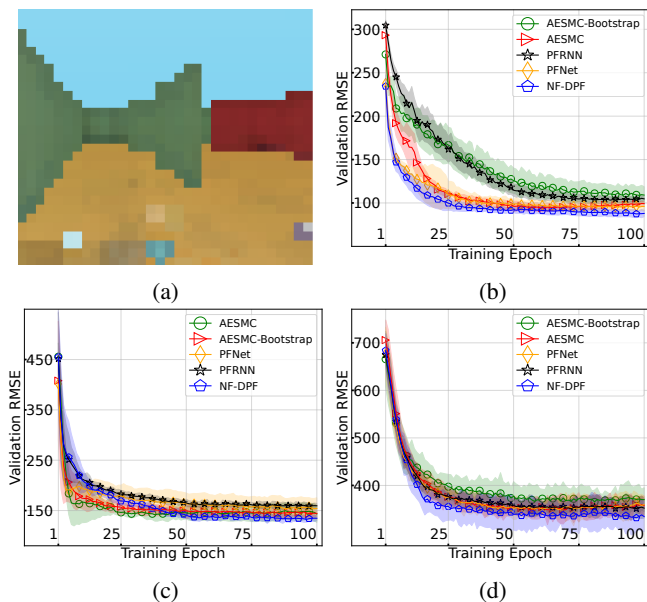


Fig. 5: (A) An example of observation images in maze environments. RMSE of different DPFs on the validation set during training in (B) Maze 1. (C) Maze 2. (D) Maze 3. The shaded area represents the standard deviation of the presented evaluation metrics among 5 random simulations.

2) *Experimental results*: We first show validation RMSEs of tested methods in Figs. 5b, 5c, and 5d. Since the size of environments varies from maze to maze (Maze 1:

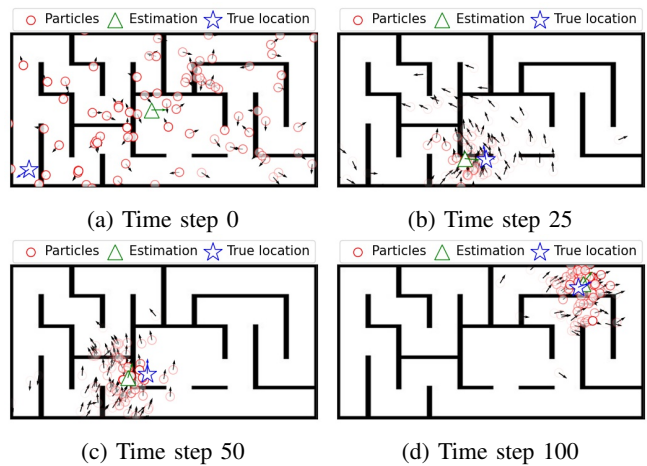


Fig. 6: A visualisation of the localisation results of the NF-DPF at different time steps. Arrows represent the orientation  $\varrho_t$  of particles and robots. The deeper the colour of a particle, the higher its importance weight.

500×1000, Maze 2: 900×1500, Maze 3: 1300×2000), the reported RMSEs increase as the maze gets larger. As expected, the proposed NF-DPF outperformed the other differentiable particle filtering frameworks regarding validation RMSEs in all three maze environments when the training has finished. In Table IV, we report the RMSE of different methods at the last time step  $t = 100$  on the test set. Experimental results shown in Table IV illustrate the superior performance of the proposed NF-DPF compared with the baseline methods. Specifically, the NF-DPF has the lowest RMSEs at the last time step in all three maze environments, implying that the NF-DPF can better localise the object for longer sequences.

TABLE IV: Test RMSE of different DPFs in maze environments. The reported RMSE is computed at the last step  $t = 100$  for 100 trajectories in the test set. Standard deviations are computed with 5 simulation runs with different random seeds.

	Method				
	AESMC Bootstrap	AESMC	PFNet	PFRNN	NF-DPF
Maze 1	56.5±11.5	52.1±7.5	51.4±8.7	54.1±8.9	<b>46.1±6.9</b>
Maze 2	115.6±6.8	109.2±11.7	120.3±8.0	125.1±8.2	<b>103.2±10.8</b>
Maze 3	220.6±11.1	201.3±14.7	212.1±15.3	210.5±10.8	<b>182.2±19.9</b>

We provide a visualisation of the localisation results in Fig. 6, where the particles, true robot locations, and estimated robot locations at different time steps are visualised. Fig. 6a shows the localisation result at the initialisation step  $t = 0$ . We can see that in Fig. 6a, the estimation is located around the centre of the maze and is far from the true location, which is expected because the particles are uniformly initialised at time step  $t = 0$ . In Fig. 6b, Fig. 6c, and Fig. 6d, it can be found that in later time steps, the NF-DPF can produce estimated locations that are close to the ground-truth locations, with particles centred at the ground-truth locations. In addition, we also observe that the learned measurement model can capture the relationship between observation images  $y_t$  and robot

locations  $x_t$ . In Fig. 6, especially Fig. 6d, it is obvious that particles that are close to the true robot location are assigned greater importance weights, and vice versa.

## VII. CONCLUSION

This paper introduced a novel variant of differentiable particle filters (DPFs), the normalising flow-based differentiable particle filter (NF-DPF), which is built based on normalising flows and conditional normalising flows. The proposed NF-DPF first provides a general mechanism to construct data-adaptive dynamic models, proposal distributions, and measurement models, three of the core components of particle filters. The theoretical analysis shows the consistency of the proposed NF-DPF and derives an upper bound for its estimation error. We empirically showed the superior performance of the NF-DPF over the other DPF methods on a wide range of simulated tasks, including parameter learning and posterior approximation in linear Gaussian state-space models, image-based disk tracking, and robot localisation in maze environments. Experimental results show that the NF-DPF can achieve the lowest tracking and localisation errors in all considered experiments, indicating that (conditional) normalising flows can indeed improve the performance of DPFs in various settings. Interesting future research directions include the development of differentiable resampling techniques with better statistical properties.

## REFERENCES

- [1] A. Doucet, A. M. Johansen *et al.*, “A tutorial on particle filtering and smoothing: Fifteen years later,” *Handb. Nonlinear Filter.*, vol. 12, no. 656–704, p. 3, 2009.
- [2] N. Gordon, D. Salmond, and A. Smith, “Novel approach to nonlinear/non-Gaussian Bayesian state estimation,” in *IEE Proc. F (Radar and Signal Process.)*, vol. 140, 1993, pp. 107–113.
- [3] P. M. Djurić, J. H. Kotecha, J. Zhang, Y. Huang, T. Ghirmai, M. F. Bugallo, and J. Míguez, “Particle filtering,” *IEEE Signal Process. Mag.*, vol. 20, no. 5, pp. 19–38, 2003.
- [4] P. Del Moral and L. Miclo, “Branching and interacting particle systems. approximations of Feynman-Kac formulae with applications to nonlinear filtering,” *Sémin. Probab. Strasbourg*, vol. 34, pp. 1–145, 2000.
- [5] D. Crisan and A. Doucet, “A survey of convergence results on particle filtering methods for practitioners,” *IEEE Trans. Signal Process.*, vol. 50, no. 3, pp. 736–746, 2002.
- [6] P. Del Moral, “Measure-valued processes and interacting particle systems. application to nonlinear filtering problems,” *Ann. Appl. Probab.*, vol. 8, no. 2, pp. 438–495, 1998.
- [7] V. Elvira, J. Míguez, and P. M. Djurić, “Adapting the number of particles in sequential Monte Carlo methods through an online scheme for convergence assessment,” *IEEE Trans. Signal Process.*, vol. 65, no. 7, pp. 1781–1794, 2017.
- [8] V. Elvira, J. Míguez, and P. M. Djurić, “On the performance of particle filters with adaptive number of particles,” *Stat. Comput.*, vol. 31, pp. 1–18, 2021.
- [9] A. Giremus, J.-Y. Tournier, and V. Calmettes, “A particle filtering approach for joint detection/estimation of multipath effects on GPS measurements,” *IEEE Trans. Signal Process.*, vol. 55, no. 4, pp. 1275–1285, 2007.
- [10] T. Zhang, C. Xu, and M.-H. Yang, “Multi-task correlation particle filter for robust object tracking,” in *Proc. IEEE Conf. Comput. Vis. and Pattern Recogn. (CVPR)*, Honolulu, Hawaii, July 2017.
- [11] D. Creal, “A survey of sequential monte carlo methods for economics and finance,” *Econometric Rev.*, vol. 31, no. 3, pp. 245–296, 2012.
- [12] X. Ma *et al.*, “Discriminative particle filter reinforcement learning for complex partial observations,” in *Proc. Int. Conf. Learn. Rep. (ICLR)*, New Orleans, USA, May 2019.
- [13] M. K. Pitt and N. Shephard, “Filtering via simulation: Auxiliary particle filters,” *J. Amer. Statist. Assoc.*, vol. 94, no. 446, pp. 590–599, 1999.
- [14] V. Elvira, L. Martino, M. F. Bugallo, and P. M. Djurić, “Elucidating the auxiliary particle filter via multiple importance sampling,” *IEEE Signal Process. Mag.*, vol. 36, no. 6, pp. 145–152, 2019.
- [15] N. Branchini and V. Elvira, “Optimized auxiliary particle filters: adapting mixture proposals via convex optimization,” in *Proc. Conf. Uncertain. Artif. Intell. (UAI)*, 2021, pp. 1289–1299.
- [16] A. Doucet, N. de Freitas, K. Murphy, and S. Russell, “Rao-Blackwellised particle filtering for dynamic Bayesian networks,” in *Proc. Conf. Uncertain. Artif. Intell. (UAI)*, Stanford, USA, 2000, pp. 176–183.
- [17] N. De Freitas, “Rao-Blackwellised particle filtering for fault diagnosis,” in *Proc. IEEE Aerosp. Conf.*, vol. 4, 2002, pp. 4–4.
- [18] A. Doucet, N. De Freitas *et al.*, *Sequential Monte Carlo methods in practice*. Springer, 2001, vol. 1, no. 2.
- [19] S. Godsill, “Particle filtering: the first 25 years and beyond,” in *Proc. IEEE Int. Conf. Acoust. Speech Signal Process. (ICASSP)*, Brighton, UK, May 2019.
- [20] R. Van Der Merwe, A. Doucet, N. De Freitas, and E. Wan, “The unscented particle filter,” *Proc. Adv. Neur. Inf. Process. Sys. (NeurIPS)*, Dec. 2000.
- [21] S. J. Julier and J. K. Uhlmann, “Unscented filtering and nonlinear estimation,” *Proc. IEEE*, vol. 92, no. 3, pp. 401–422, 2004.
- [22] N. Oudjane and C. Musso, “Progressive correction for regularized particle filters,” in *Proc. IEEE Int. Conf. Inf. Fusion (FUSION)*, Paris, France, July 2000.
- [23] C. Musso, N. Oudjane, and F. Le Gland, “Improving regularised particle filters,” *Sequential Monte Carlo methods in practice*, pp. 247–271, 2001.
- [24] P. M. Djurić, T. Lu, and M. F. Bugallo, “Multiple particle filtering,” in *Proc. IEEE Int. Conf. Acoust. Speech Signal Process. (ICASSP)*, Honolulu, USA, Apr. 2007.
- [25] P. M. Djurić and M. F. Bugallo, “Particle filtering for high-dimensional systems,” in *Proc. Comput. Adv. Multi-Sensor Adapt. Process. (CAM-SAP)*, Saint Martin, France, Dec. 2013.
- [26] J. H. Kotecha and P. M. Djurić, “Gaussian sum particle filtering for dynamic state-space models,” in *Proc. IEEE Int. Conf. Acoust. Speech Signal Process.*, Salt Lake City, USA, May 2001.
- [27] —, “Gaussian sum particle filtering,” *IEEE Trans. Signal Process.*, vol. 51, no. 10, pp. 2602–2612, 2003.
- [28] N. Kantas, A. Doucet, S. S. Singh, J. Maciejowski, and N. Chopin, “On particle methods for parameter estimation in state-space models,” *Stat. Sci.*, vol. 30, no. 3, pp. 328–351, 2015.
- [29] N. Kantas, A. Doucet, S. S. Singh, and J. M. Maciejowski, “An overview of sequential Monte Carlo methods for parameter estimation in general state-space models,” *IFAC Proc. Vol.*, vol. 42, no. 10, pp. 774–785, 2009.
- [30] M. Hürzeler and H. R. Künsch, “Approximating and maximising the likelihood for a general state-space model,” *Sequential Monte Carlo methods in practice*, pp. 159–175, 2001.
- [31] E. L. Ionides, C. Bretó, and A. A. King, “Inference for nonlinear dynamical systems,” *Proc. Natl. Acad. Sci.*, vol. 103, no. 49, pp. 18438–18443, 2006.
- [32] S. Malik and M. K. Pitt, “Particle filters for continuous likelihood evaluation and maximisation,” *J. Econometrics*, vol. 165, no. 2, pp. 190–209, 2011.
- [33] J. Olsson, O. Cappé, R. Douc, and É. Moulines, “Sequential Monte Carlo smoothing with application to parameter estimation in nonlinear state space models,” *Bernoulli*, vol. 14, no. 1, pp. 155–179, 2008.
- [34] G. Poyiadjis, A. Doucet, and S. S. Singh, “Particle approximations of the score and observed information matrix in state space models with application to parameter estimation,” *Biometrika*, vol. 98, no. 1, pp. 65–80, 2011.
- [35] C. Andrieu, A. Doucet, and R. Holenstein, “Particle markov chain monte carlo methods,” *J. R. Stat. Soc. Ser. B. Stat. Methodol.*, vol. 72, no. 3, pp. 269–342, 2010.
- [36] N. Chopin, P. E. Jacob, and O. Papaspiliopoulos, “SMC2: an efficient algorithm for sequential analysis of state space models,” *J. R. Stat. Soc. Ser. B. Stat. Methodol.*, vol. 75, no. 3, pp. 397–426, 2013.
- [37] S. Pérez-Vieites, I. P. Mariño, and J. Míguez, “Probabilistic scheme for joint parameter estimation and state prediction in complex dynamical systems,” *Phys. Rev. E*, vol. 98, no. 6, p. 063305, 2018.
- [38] F. Lindsten, M. I. Jordan, and T. B. Schon, “Particle gibbs with ancestor sampling,” *J. Mach. Learn. Res.*, vol. 15, pp. 2145–2184, 2014.
- [39] X. Chen and Y. Li, “An overview of differentiable particle filters for data-adaptive sequential Bayesian inference,” *arXiv preprint arXiv:2302.09639*, 2023.
- [40] R. Jonschkowski, D. Rastogi, and O. Brock, “Differentiable particle filters: end-to-end learning with algorithmic priors,” in *Proc. Robot. Sci. and Syst. (RSS)*, Pittsburgh, Pennsylvania, July 2018.

- [41] P. Karkus, D. Hsu, and W. S. Lee, "Particle filter networks with application to visual localization," in *Proc. Conf. Robot Learn. (CoRL)*, Zurich, Switzerland, Oct 2018.
- [42] A. Corenflos, J. Thornton, G. Deligiannidis, and A. Doucet, "Differentiable particle filtering via entropy-regularized optimal transport," in *Proc. Int. Conf. Mach. Learn. (ICML)*, July 2021.
- [43] A. Ścibior and F. Wood, "Differentiable particle filtering without modifying the forward pass," *arXiv preprint arXiv:2106.10314*, 2021.
- [44] A. Kloss, G. Martius, and J. Bohg, "How to train your differentiable filter," *Auto. Robot.*, vol. 45, no. 4, pp. 561–578, 2021.
- [45] M. Zhu, K. Murphy, and R. Jonschkowski, "Towards differentiable resampling," *arXiv preprint arXiv:2004.11938*, 2020.
- [46] T. A. Le, M. Igl, T. Rainforth, T. Jin, and F. Wood, "Auto-encoding sequential Monte Carlo," in *Proc. Int. Conf. Learn. Rep. (ICLR)*, Vancouver, Canada, Apr. 2018.
- [47] C. Naesseth, S. Linderman, R. Ranganath, and D. Blei, "Variational sequential Monte Carlo," in *Proc. Int. Conf. Artif. Intel. and Stat. (AISTATS)*, Playa Blanca, Spain, Apr. 2018.
- [48] C. J. Maddison *et al.*, "Filtering variational objectives," in *Proc. Adv. Neur. Inf. Process. Sys. (NeurIPS)*, Long Beach, USA, Dec. 2017.
- [49] P. Bickel, B. Li, and T. Bengtsson, "Sharp failure rates for the bootstrap particle filter in high dimensions," *Pushing the limits of contemporary statistics: Contributions in honor of Jayanta K. Ghosh*, 2008.
- [50] X. Chen, H. Wen, and Y. Li, "Differentiable particle filters through conditional normalizing flow," in *Proc. IEEE Int. Conf. Inf. Fusion (FUSION)*, Sun City, South Africa, Nov. 2021.
- [51] X. Chen and Y. Li, "Conditional measurement density estimation in sequential Monte Carlo via normalizing flow," in *Proc. Euro. Sig. Process. Conf. (EUSIPCO)*, Belgrade, Serbia, Aug. 2022.
- [52] E. L. IONIDES, A. BHADRA, Y. ATCHADÉ, and A. KING, "Iterated filtering," *Ann. of Statist.*, vol. 39, no. 3, pp. 1776–1802, 2011.
- [53] Z. Zhao, B. Huang, and F. Liu, "Parameter estimation in batch process using EM algorithm with particle filter," *Comput. & Chem. Eng.*, vol. 57, pp. 159–172, 2013.
- [54] A. Wills, T. B. Schön, and B. Ninness, "Parameter estimation for discrete-time nonlinear systems using EM," *IFAC Proc. Vol.*, vol. 41, no. 2, pp. 4012–4017, 2008.
- [55] C. Andrieu, A. Doucet, and V. B. Tadic, "On-line parameter estimation in general state-space models," in *Proc. IEEE Conf. Dec. and Contr. (CDC)*, Seville, Spain, Dec. 2005.
- [56] F. LeGland and L. Mével, "Recursive estimation in hidden markov models," in *Proc. IEEE Conf. Decis. Control (CDC)*, vol. 4. IEEE, 1997, pp. 3468–3473.
- [57] D. Crisan and J. Míguez, "Nested particle filters for online parameter estimation in discrete-time state-space Markov models," *Bernoulli*, vol. 24, no. 4A, pp. 3039–3086, 2018.
- [58] S. Pérez-Vicites and J. Míguez, "Nested Gaussian filters for recursive Bayesian inference and nonlinear tracking in state space models," *Signal Proces.*, vol. 189, p. 108295, 2021.
- [59] N. G. Polson, J. R. Stroud, and P. Müller, "Practical filtering with sequential parameter learning," *J. R. Stat. Soc. Ser. B. Stat. Methodol.*, vol. 70, no. 2, pp. 413–428, 2008.
- [60] J. Fernández-Villaverde and J. F. Rubio-Ramírez, "Estimating macroeconomic models: A likelihood approach," *Rev. Econ. Stud.*, vol. 74, no. 4, pp. 1059–1087, 2007.
- [61] N. Chopin, "Central limit theorem for sequential Monte Carlo methods and its application to bayesian inference," *Ann. Statist.*, vol. 32, no. 6, pp. 2385–2411, 2004.
- [62] C. Rosato, L. Devlin, V. Beraud, P. Horridge, T. B. Schön, and S. Maskell, "Efficient learning of the parameters of non-linear models using differentiable resampling in particle filters," *IEEE Trans. Signal Process. (TSP)*, vol. 70, pp. 3676–3692, 2022.
- [63] X. Ma, P. Karkus, D. Hsu, and W. S. Lee, "Particle filter recurrent neural networks," in *Proc. AAAI Conf. Artif. Intell. (AAAI)*, New York, USA, Feb. 2020.
- [64] M. Cuturi, "Sinkhorn distances: Lightspeed computation of optimal transport," in *Proc. Adv. Neur. Inf. Process. Sys. (NeurIPS)*, Lake Tahoe, USA, Dec. 2013.
- [65] J. Feydy *et al.*, "Interpolating between optimal transport and mmd using Sinkhorn divergences," in *Proc. Int. Conf. Artif. Intell. Stat. (AISTATS)*, Naha, Japan, Apr. 2019.
- [66] G. Peyré and M. Cuturi, "Computational optimal transport," *Foundations and Trends® in Machine Learning*, vol. 11, no. 5-6, pp. 355–607, 2019.
- [67] J. Lee *et al.*, "Set transformer: A framework for attention-based permutation-invariant neural networks," in *Proc. Int. Conf. Mach. Learn. (ICML)*, Baltimore, USA, June 2019.
- [68] A. Vaswani *et al.*, "Attention is all you need," in *Proc. Adv. Neur. Inf. Process. Sys. (NeurIPS)*, Long Beach, USA, Dec. 2017.
- [69] M. H. Dupty, Y. Dong, and W. S. Lee, "PF-GNN: Differentiable particle filtering based approximation of universal graph representations," in *Proc. Int. Conf. Learn. Rep. (ICLR)*, May 2021.
- [70] R. Chen, H. Yin, Y. Jiao, G. Dissanayake, Y. Wang, and R. Xiong, "Deep samplable observation model for global localization and kidnapping," *IEEE Robot. Autom. Lett. (RAL)*, vol. 6, no. 2, pp. 2296–2303, 2021.
- [71] A. Doucet, D. N. Freitas, and N. Gordon, "An introduction to sequential Monte Carlo methods," in *Sequential Monte Carlo methods in practice*. Springer, 2001, pp. 3–14.
- [72] R. E. Kalman, "A new approach to linear filtering and prediction problems," *J. Basic Eng.*, vol. 82, no. 1, pp. 33–45, 1960.
- [73] R. Douc and O. Cappé, "Comparison of resampling schemes for particle filtering," in *Proc. Int. Symp. Image and Signal Process. and Anal.*, Zagreb, Croatia, 2005.
- [74] T. Li, M. Bolic, and P. M. Djuric, "Resampling methods for particle filtering: classification, implementation, and strategies," *IEEE Signal Process. Mag.*, vol. 32, no. 3, pp. 70–86, 2015.
- [75] I. Kobyzev, S. Prince, and M. Brubaker, "Normalizing flows: An introduction and review of current methods," *IEEE Trans. Pattern Anal. Mach. Intell. (TPAMI)*, vol. 43, no. 11, pp. 3964–3979, 2020.
- [76] G. Papamakarios, E. Nalisnick, D. J. Rezende, S. Mohamed, and B. Lakshminarayanan, "Normalizing flows for probabilistic modeling and inference," *J. Mach. Learn. Res.*, vol. 22, pp. 1–64, 2021.
- [77] L. Dinh, J. Sohl-Dickstein, and S. Bengio, "Density estimation using Real NVP," in *Proc. Int. Conf. Learn. Represent. (ICLR)*, Toulon, France, Apr. 2017.
- [78] M. Balunovic, A. Ruoss, and M. Vechev, "Fair normalizing flows," in *Proc. Int. Conf. Learn. Represent. (ICLR)*, Apr. 2022.
- [79] D. P. Kingma and P. Dhariwal, "Glow: Generative flow with invertible 1x1 convolutions," in *Proc. Adv. Neur. Inf. Process. Sys. (NeurIPS)*, Montreal, Canada, Dec. 2018.
- [80] D. Rezende and S. Mohamed, "Variational inference with normalizing flows," in *Proc. Int. Conf. Mach. Learn. (ICML)*, Lille, France, July 2015.
- [81] M. Karami, D. Schuurmans, J. Sohl-Dickstein, L. Dinh, and D. Duckworth, "Invertible convolutional flow," in *Proc. Adv. Neur. Inf. Process. Sys. (NeurIPS)*, Vancouver, Canada, Dec. 2019.
- [82] C. Huang, D. Krueger, A. Lacoste, and A. Courville, "Neural autoregressive flows," in *Proc. Int. Conf. Mach. Learn. (ICML)*, Stockholm, Sweden, Aug. 2018.
- [83] C. Winkler, D. Worrall, E. Hoogeboom, and M. Welling, "Learning likelihoods with conditional normalizing flows," *arXiv preprint arXiv:1912.00042*, 2019.
- [84] Y. Lu and B. Huang, "Structured output learning with conditional generative flows," in *Proc. AAAI Conf. Artif. Intell. (AAAI)*, New York, USA, Feb. 2020.
- [85] C. Villani, *Optimal Transport: old and new*. Berlin, Germany: Springer Science & Business Media, 2008, vol. 338.
- [86] N. Chopin and O. Papaspiliopoulos, *An introduction to sequential Monte Carlo*. Springer, 2020.
- [87] T. Haarnoja, A. Ajay, S. Levine, and P. Abbeel, "Backprop KF: Learning discriminative deterministic state estimators," in *Proc. Adv. Neur. Inf. Process. Sys. (NeurIPS)*, Barcelona, Spain, Dec. 2016.
- [88] C. Beattie, J. Z. Leibo, D. Teplyaev, T. Ward, M. Wainwright, H. Küttler, A. Lefrancq, S. Green, V. Valdés, A. Sadik *et al.*, "Deepmind lab," *arXiv preprint arXiv:1612.03801*, 2016.
- [89] K. D. P. and B. J., "Adam: A method for stochastic optimization," in *Proc. Int. Conf. on Learn. Represent. (ICLR)*, San Diego, USA, May 2015.
- [90] N. Fournier and A. Guillin, "On the rate of convergence in Wasserstein distance of the empirical measure," *Probab. Theory Related Fields*, vol. 162, no. 3, pp. 707–738, 2015.

APPENDIX A  
OPTIMAL TRANSPORT BACKGROUND

In this section, we provide a brief review of concepts related to the proposed work, including the definition of Wasserstein distances, the optimal transport plan (coupling), and the optimal transport map. Note that notations introduced in Section V also apply in this section.

**Wasserstein Distance:**

Let  $P_p(\mathcal{X})$  be a set of Borel probability measures with a finite  $p$ -th moment on a Polish metric space  $(\mathcal{X}, d)$  [85]. Given two probability measures  $\alpha, \beta \in P_p(\mathcal{X})$ , the Wasserstein distance of order  $p \in [1, +\infty)$  between  $\alpha$  and  $\beta$  is defined as:

$$\mathcal{W}_p(\alpha, \beta) = \left( \inf_{\mathcal{P} \in \mathcal{U}(\alpha, \beta)} \int_{\mathcal{X} \times \mathcal{X}} d(x, x')^p \mathcal{P}(dx, dx') \right)^{\frac{1}{p}}, \quad (53)$$

where  $d(\cdot, \cdot)^p$  is the cost function,  $\mathcal{U}(\alpha, \beta)$  represents the set of all transportation plans  $\mathcal{P}(dx, dx')$ , i.e. joint distributions whose marginals are  $\alpha$  and  $\beta$ , respectively. Every transport plan  $\mathcal{P}(dx, dx')$  corresponds to a transport map, also called the barycentric projection map, which is defined as  $\mathbf{T}(x) = \int x' \mathcal{P}(dx'|x)$ .

**Optimal Transport Notations:**

Solving the original optimal transport problem is computationally expensive and non-differentiable, an alternative is to rely on entropy-regularised optimal transport [64], [66]. In the DPF setting,  $\epsilon$  denotes the regularisation coefficient in the entropy-regularised optimal transport problem,  $\mathcal{P}_{N, \epsilon}^{\text{OT}}$  denotes the regularised transport plan between  $\alpha_N^{(t)}$  and  $\beta_N^{(t)}$ ,  $\mathbf{T}(\cdot) : \mathcal{X} \rightarrow \mathcal{X}$  denotes the optimal transport map between  $\alpha^{(t)}$  and  $\beta^{(t)}$ , and  $\mathbf{T}_{N, \epsilon}(\cdot) : \mathcal{X} \rightarrow \mathcal{X}$ ,  $\mathbf{T}_{N, \epsilon}(x) := \int x' \mathcal{P}_{N, \epsilon}^{\text{OT}}(dx'|x)$  the transport map induced by the transport plan  $\mathcal{P}_{N, \epsilon}^{\text{OT}}$ .

APPENDIX B  
PROOF OF PROPOSITION V.1

We use notations below for the following proofs:

$$\alpha^{(t)} := p(x_t | y_{0:t-1}; \theta), \quad \beta^{(t)} := p(x_t | y_{0:t}; \theta), \quad (54)$$

$$\alpha_N^{(t)}(\psi) := \frac{1}{N} \sum_{i=1}^N \psi(x_t^i), \quad \beta_N^{(t)}(\psi) := \sum_{i=1}^N \mathbf{w}_t^i \psi(x_t^i), \quad (55)$$

$$\tilde{\beta}_N^{(t)}(\psi) := \frac{1}{N} \sum_{i=1}^N \psi(\tilde{x}_t^i), \quad \omega^{(t)}(x_t) = p(y_t | x_t; \theta), \quad (56)$$

with  $\alpha^{(0)} := \pi(x_0; \theta)$ ,  $\psi(\cdot) : \mathcal{X} \rightarrow \mathbb{R}$  is a function defined on  $\mathcal{X}$ ,  $\alpha_N^{(t)}$  is an approximation of the predictive distribution  $\alpha^t$  with  $N$  uniformly weighted particles, and  $\beta_N^{(t)}$  is an approximation of the posterior distribution  $\beta^{(t)}$  with  $N$  particles weighted by  $\mathbf{w}_t^i$ .  $\tilde{\beta}_N^{(t)}$  is an approximation of the posterior distribution  $\beta^{(t)}$  with uniformly weighted particles  $\tilde{x}_t^i$  obtained by applying the entropy-regularised optimal transport resampler in [42] as shown in the line 12 of Algorithm 1. For a measure  $\alpha$  defined on  $\mathcal{X}$  we use  $\alpha(\psi) = \int_{\mathcal{X}} \psi(x) \alpha(dx)$  to denote the expectation of  $\psi(\cdot)$  w.r.t.  $\alpha$ .

To prove Proposition V.1, we first present five Lemmas B.1, B.2, B.3, B.4, B.5 and Proposition B.1. Lemma B.3

is borrowed from [42] (Lemma C.2). The proof of Proposition V.1 is based on proof by induction, which is inspired by the proof of Proposition 11.3 of [86].

**Lemma B.1.** *For all bounded  $k$ -Lipschitz function  $\psi(\cdot) : \mathcal{X} \rightarrow \mathbb{R}$  and any two probability measures  $\mu, \rho$  on  $\mathcal{X}$ , we have:*

$$|\mu(\psi) - \rho(\psi)| \leq k \mathcal{W}_1(\mu, \rho). \quad (57)$$

*Proof.* Denote by

$$\mathcal{P}^*(dx, dx') := \operatorname{argmin}_{\mathcal{P} \in \mathcal{U}(\mu, \rho)} \int_{\mathcal{X}^2} \|x - x'\|_2 \mathcal{P}(dx, dx')$$

the optimal transport plan between  $\mu$  and  $\rho$  w.r.t. the Euclidean distance, we have:

$$\begin{aligned} & |\mu(\psi) - \rho(\psi)| \\ &= \left| \int_{\mathcal{X}} \psi(x) \mu(dx) - \int_{\mathcal{X}} \psi(x') \rho(dx') \right| \\ &= \left| \int_{\mathcal{X}^2} \psi(x) \mathcal{P}^*(dx, dx') - \int_{\mathcal{X}^2} \psi(x') \mathcal{P}^*(dx, dx') \right| \\ &\leq \int_{\mathcal{X}^2} |\psi(x) - \psi(x')| \mathcal{P}^*(dx, dx') \\ &\leq \int_{\mathcal{X}^2} k \|x - x'\|_2 \mathcal{P}^*(dx, dx') \\ &= k \mathcal{W}_1(\mu, \rho). \end{aligned} \quad (58)$$

□

**Lemma B.2.** *For probability measures  $\mu$  and  $\rho$  defined on  $\mathcal{X}$ , denote by  $\mathbf{T}(\cdot) : \mathcal{X} \rightarrow \mathcal{X}$  the optimal transport map between them. Let  $\mu_N = \sum_{i=1}^N a_i \delta_{x_i'}$  and  $\rho_N = \sum_{j=1}^M b_j \delta_{x_j}$  be approximations of  $\mu$  and  $\rho$ , where  $x_i' \in \mathcal{X}$  and  $x_j \in \mathcal{X}$  for  $\forall i, j \in \{1, \dots, N\}$ . Denote by  $\mathcal{P}_N(dx', dx) \in \mathcal{U}(\mu_N, \rho_N)$  a transport plan between  $\mu_N$  and  $\rho_N$ , and  $\mathbf{T}_N(\cdot) : \mathcal{X} \rightarrow \mathcal{X}$  the transport map induced by  $\mathcal{P}_N(dx', dx)$ , namely  $\mathbf{T}_N(x_i') = \frac{1}{a_i} \sum_{j=1}^M p_{i,j} x_j$  with  $p_{i,j} = \mathcal{P}_{N,i,j}$  the element at the intersection of  $\mathcal{P}_N$ 's  $i$ -th row and  $j$ -th column. The following inequality holds:*

$$\begin{aligned} & \int_{\mathcal{X}^2} \|\mathbf{T}(x) - \mathbf{T}_N(x)\|^2 \mathcal{P}_N(dx', dx) \\ & \leq \int_{\mathcal{X}^2} \|\mathbf{T}(x') - x\|^2 \mathcal{P}_N(dx', dx) \end{aligned} \quad (60)$$

*Proof.* Firstly, denote by  $\langle \cdot, \cdot \rangle$  the inner product operation, we have that:

$$\begin{aligned} \sum_{i=1}^N \sum_{j=1}^M p_{i,j} \langle \mathbf{T}(x_i'), x_j \rangle &= \sum_{i=1}^N a_i \langle \mathbf{T}(x_i'), \mathbf{T}_N(x_i') \rangle \\ &= \sum_{i=1}^N \sum_{j=1}^M p_{i,j} \langle \mathbf{T}(x_i'), \mathbf{T}_N(x_i') \rangle, \end{aligned} \quad (61)$$

$$\begin{aligned} \sum_{i=1}^N \sum_{j=1}^M p_{i,j} \langle \mathbf{T}_N(x_i'), x_j \rangle &= \sum_{i=1}^N a_i \langle \mathbf{T}_N(x_i'), \mathbf{T}_N(x_i') \rangle \\ &= \sum_{i=1}^N \sum_{j=1}^M p_{i,j} \langle \mathbf{T}_N(x_i'), \mathbf{T}_N(x_i') \rangle. \end{aligned} \quad (62)$$

The above equation leads to:

$$\sum_{i=1}^N \sum_{j=1}^M p_{i,j} \|\mathbf{T}(x'_i) - x_j\|^2 \quad (63)$$

$$= \sum_{i=1}^N \sum_{j=1}^M p_{i,j} \left\langle (\mathbf{T}(x'_i) - x_j), (\mathbf{T}(x'_i) - x_j) \right\rangle \quad (64)$$

$$= \sum_{i=1}^N \sum_{j=1}^M p_{i,j} \left( \left\langle \mathbf{T}(x'_i), \mathbf{T}(x'_i) \right\rangle + \left\langle \mathbf{T}_N(x'_i), \mathbf{T}_N(x'_i) \right\rangle \right. \\ \left. - 2 \left\langle \mathbf{T}(x'_i), \mathbf{T}_N(x'_i) \right\rangle + \left\langle \mathbf{T}_N(x'_i), \mathbf{T}_N(x'_i) \right\rangle \right. \\ \left. + \left\langle x_j, x_j \right\rangle - 2 \left\langle \mathbf{T}_N(x'_i), x_j \right\rangle \right) \quad (66)$$

$$= \sum_{i=1}^N \sum_{j=1}^M p_{i,j} \left( \|\mathbf{T}(x'_i) - \mathbf{T}_N(x'_i)\|^2 + \|\mathbf{T}_N(x'_i) - x_j\|^2 \right) \quad (67)$$

$$\geq \sum_{i=1}^N \sum_{j=1}^M p_{i,j} \left( \|\mathbf{T}(x'_i) - \mathbf{T}_N(x'_i)\|^2 \right). \quad (68)$$

Therefore the stated result is obtained:

$$\int_{\mathcal{X}^2} \|\mathbf{T}(x') - \mathbf{T}_N(x')\|^2 \mathcal{P}_N(dx', dx) \quad (69)$$

$$= \sum_{i=1}^N \sum_{j=1}^M p_{i,j} \|\mathbf{T}(x'_i) - \mathbf{T}_N(x'_i)\|^2 \quad (70)$$

$$\leq \sum_{i=1}^N \sum_{j=1}^M p_{i,j} \|\mathbf{T}(x'_i) - x_j\|^2 \quad (71)$$

$$= \int_{\mathcal{X}^2} \|\mathbf{T}(x') - x\|^2 \mathcal{P}_N(dx', dx). \quad (72)$$

□

**Lemma B.3.** (Lemma C.2 in [42]) *Let  $\mathcal{X} \subset \mathbb{R}^d$  be compact with diameter  $\mathfrak{d} > 0$ . Suppose we are given two probability measures  $\alpha, \beta$  on  $\mathcal{X}$  with a unique deterministic,  $\lambda$ -Lipschitz optimal transport map  $\mathbf{T}$  while  $\alpha_N = \sum_{i=1}^N a_i \delta_{x'_i}$  with  $a_i > 0$  and  $\beta_N = \sum_{i=1}^N b_i \delta_{x_i}$ . We write  $\mathcal{P}_{N,\epsilon}^{\text{OT},N}$ , resp.  $\mathcal{P}_{N,\epsilon}^{\text{OT},N}$ , for an optimal coupling between  $\alpha_N$  and  $\beta_N$ , resp. the  $\epsilon$ -regularized optimal transport plan, between  $\alpha_N$  and  $\beta_N$ . Then*

$$\left[ \int \|x - \mathbf{T}(x')\|^2 \mathcal{P}_{N,\epsilon}^{\text{OT}}(dx', dx) \right]^{\frac{1}{2}} \leq 2\lambda^{1/2} \mathcal{E}^{1/2} [\mathfrak{d} + \mathcal{E}]^{1/2} \\ + \max\{\lambda, 1\} [\mathcal{W}_2(\alpha_N, \alpha) + \mathcal{W}_2(\beta_N, \beta)],$$

where

$$\mathcal{E} := \mathcal{E}(N, \epsilon, \alpha, \beta) := \mathcal{W}_2(\alpha_N, \alpha) + \mathcal{W}_2(\beta_N, \beta) + \sqrt{2\epsilon \log(N)}.$$

**Proposition B.1.** *Consider atomic probability measures  $\alpha_N = \sum_{i=1}^N a_i \delta_{x'_i}$  with  $a_i > 0$  and  $\beta_N = \sum_{i=1}^N b_i \delta_{x_i}$ , with support  $\mathcal{X} \subset \mathbb{R}^d$ . Denote by  $\mathcal{P}_{N,\epsilon,i,j}^{\text{OT}}$  the element at the intersection of  $i$ -th row and  $j$ -th column of the  $\epsilon$ -regularized optimal transport coupling  $\mathcal{P}_{N,\epsilon}^{\text{OT}}$  between  $\alpha_N$  and  $\beta_N$ , and define  $\tilde{\beta}_N = \sum_{i=1}^N a_i \delta_{\tilde{x}_{i,N,\epsilon}}$ , where  $\tilde{x}_{i,N,\epsilon} = \frac{1}{a_i} \sum_{j=1}^N \mathcal{P}_{N,\epsilon,i,j}^{\text{OT}} x_j$ . Let  $\alpha, \beta$  be two other probability measures, also supported on  $\mathcal{X}$ , such that there exists a unique  $\lambda$ -Lipschitz optimal transport*

*map  $\mathbf{T}(\cdot) : \mathcal{X} \rightarrow \mathcal{X}$  between them. Then for any bounded  $k$ -Lipschitz function  $\psi(\cdot) : \mathcal{X} \rightarrow \mathbb{R}$ , we have*

$$\left| \beta_N(\psi) - \tilde{\beta}_N(\psi) \right| \leq \sqrt{2}k \left( 2\lambda^{1/2} \mathcal{E}^{1/2} [\mathfrak{d} + \mathcal{E}]^{1/2} \right. \\ \left. + \max\{\lambda, 1\} [\mathcal{W}_2(\alpha_N, \alpha) + \mathcal{W}_2(\beta_N, \beta)] \right), \quad (73)$$

where  $\mathfrak{d} := \sup_{x, x' \in \mathcal{X}} \|x - x'\|_2$  and  $\mathcal{E} = \mathcal{W}_2(\alpha_N, \alpha) + \mathcal{W}_2(\beta_N, \beta) + \sqrt{2\epsilon \log N}$ .

*Proof.* By definition, we have  $\tilde{\beta}_N(d\tilde{x}) = \int \alpha_N(dx') \delta_{\mathbf{T}_{N,\epsilon}(x')}(d\tilde{x})$  with  $\mathbf{T}_{N,\epsilon}(x') := \int x \mathcal{P}_{N,\epsilon}^{\text{OT}}(dx|x')$  while, as  $\mathcal{P}_{N,\epsilon}^{\text{OT}}$  belongs to  $\mathcal{U}(\alpha_N, \beta_N)$ , we also have  $\beta_N(dx) = \int \alpha_N(dx') \mathcal{P}_{N,\epsilon}^{\text{OT}}(dx|x')$ . We then have for any 1-Lipschitz function

$$\left| \beta_N(\psi) - \tilde{\beta}_N(\psi) \right| \\ = \left| \int \left[ \int (\psi(x) - \psi(\mathbf{T}_{N,\epsilon}(x'))) \mathcal{P}_{N,\epsilon}^{\text{OT}}(dx|x') \right] \alpha_N(dx') \right| \\ \leq \int \int |\psi(x) - \psi(\mathbf{T}_{N,\epsilon}(x'))| \alpha_N(dx') \mathcal{P}_{N,\epsilon}^{\text{OT}}(dx|x') \\ \leq k \int \int \|x - \mathbf{T}_{N,\epsilon}(x')\| \mathcal{P}_{N,\epsilon}^{\text{OT}}(dx', dx) \\ \leq k \left( \int \int \|x - \mathbf{T}_{N,\epsilon}(x')\|^2 \mathcal{P}_{N,\epsilon}^{\text{OT}}(dx', dx) \right)^{\frac{1}{2}} \\ \leq k \left( \int \int (\|x - \mathbf{T}(x')\|^2 + \|\mathbf{T}(x') - \mathbf{T}_{N,\epsilon}(x')\|^2) \mathcal{P}_{N,\epsilon}^{\text{OT}}(dx', dx) \right)^{\frac{1}{2}} \\ \leq \sqrt{2}k \left( \int \int \|x - \mathbf{T}(x')\|^2 \mathcal{P}_{N,\epsilon}^{\text{OT}}(dx', dx) \right)^{\frac{1}{2}},$$

where the final inequality follows from Lemma B.2. The stated result is then obtained using Lemma B.3. □

**Lemma B.4.** *For all bounded  $k$ -Lipschitz function  $\psi(\cdot) : \mathcal{X} \rightarrow \mathbb{R}$ , when the entropy-regularisation hyperparameter  $\epsilon_N = o(1/\log N)$ , for  $\alpha_N^{(t)}, \beta_N^{(t-1)}$  defined as in Eq. (55), and transition kernel  $f(\cdot)$  defined by  $p(x_t|x_{t-1}; \theta)$  in Eq. (17), the expectations  $\alpha_N^{(t)}(\psi)$  and  $\beta_N^{(t-1)}(\psi)$  satisfy:*

$$\mathbb{E} \left[ \left( \alpha_N^{(t)}(\psi) - \beta_N^{(t-1)}(\psi) \right)^2 \right] \leq \mathcal{C} \|\psi\|_\infty^2, \quad (74)$$

where

$$\mathcal{C} := \mathcal{C}(\lambda, k, \eta, \zeta, \tau, N, p, q, d_{\mathcal{X}}) \quad (75)$$

$$= 4k\sqrt{\mathcal{Q}} + 4\sqrt{2}k\eta \left( 2\sqrt{3\lambda(1+\zeta)\tau\sqrt{\mathcal{Q}}} \right) \quad (76)$$

$$+ \max\{\lambda, 1\} (1 + \zeta) \sqrt{\mathcal{Q}}, \quad (77)$$

is a constant depending on  $\lambda, k, \eta, \zeta, \tau, N, p, q, d_{\mathcal{X}}$ . The function  $\mathcal{Q}$  is defined as  $\mathcal{Q} := \mathcal{Q}(\tau, N, p, d_{\mathcal{X}}, q) :=$

$C_1 \tau^p \mathcal{H}(N, p, d_{\mathcal{X}}, q)$ ,  $C_1$  is a constant depending only on  $p$ ,  $d_{\mathcal{X}}$ ,  $q$ , and  $\mathcal{H}(N, p, d_{\mathcal{X}}, q)$  is defined as

$$\mathcal{H}(N, p, d_{\mathcal{X}}, q) = \begin{cases} N^{-1/2} + N^{-(q-p)/q} & \text{if } p > d_{\mathcal{X}}/2 \\ & \text{and } q \neq 2p, \\ N^{-1/2} \log(1+N) + N^{-(q-p)/q} & \text{if } p = d_{\mathcal{X}}/2 \\ & \text{and } q \neq 2p, \\ N^{-p/d_{\mathcal{X}}} + N^{-(q-p)/q} & \text{if } p \in (0, d_{\mathcal{X}}/2) \\ & \text{and } q \neq d_{\mathcal{X}}/(d_{\mathcal{X}} - p), \end{cases} \quad (78)$$

where  $q > p$  is a constant satisfying  $\int_{\mathcal{X}} |x|^q \alpha'_N{}^{(t)}(dx) < \infty$  and  $\int_{\mathcal{X}} |x|^q \alpha'^{(t-1)}(dx) < \infty$ ,  $p = 2$  is the order of Wasserstein distances as detailed in the proof, and  $\tau = \frac{\mathfrak{d}}{\|\psi\|_{\infty}}$ . Besides, for large enough  $N$  and  $d_{\mathcal{X}}$  such that  $\mathcal{Q} \leq \sqrt{\mathcal{Q}} \leq \sqrt[4]{\mathcal{Q}}$  and  $\mathcal{H}(N, p, d_{\mathcal{X}}, q) = N^{-p/d_{\mathcal{X}}} + N^{-(q-p)/q} \leq 2N^{-p/d_{\mathcal{X}}}$ , we also have that:

$$\mathbb{E} \left[ \left( \alpha'_N{}^{(t)}(\psi) - \beta_N^{(t-1)} f(\psi) \right)^2 \right] \leq \frac{\tilde{\mathcal{C}} \|\psi\|_{\infty}^2}{N^{1/2d_{\mathcal{X}}}}, \quad (79)$$

where

$$\tilde{\mathcal{C}} := \tilde{\mathcal{C}}(\lambda, k, \eta, \mathfrak{d}, \tau, N, p, q, d_{\mathcal{X}}) \quad (80)$$

$$:= 4k \sqrt[4]{2C_1 \mathfrak{d}^2} \left( 1 + \sqrt{2\eta} \left( 2\sqrt{3\lambda(1+\zeta)\tau} \right. \right. \quad (81)$$

$$\left. \left. + \max\{\lambda, 1\}(1+\zeta) \right) \right) \quad (82)$$

is a constant.

*Proof.* We first decompose  $\alpha'_N{}^{(t)}(\psi) - \beta_N^{(t-1)} f(\psi)$  into two terms:

$$\alpha'_N{}^{(t)}(\psi) - \beta_N^{(t-1)} f(\psi) \quad (83)$$

$$= \left( \alpha'_N{}^{(t)}(\psi) - \alpha'_N{}^{(t)}(\psi) \right) + \left( \alpha'_N{}^{(t)}(\psi) - \beta_N^{(t-1)} f(\psi) \right), \quad (84)$$

where  $\alpha'_N{}^{(t)}$  is defined as  $\alpha'_N{}^{(t)} := \tilde{\beta}_N^{(t-1)} f$ . The first term in Eq. (83) can be bounded by applying Lemma B.1 to probability measures  $\alpha_N^{(t)}(\psi)$  and  $\alpha'_N{}^{(t)}(\psi)$ :

$$\left| \alpha'_N{}^{(t)}(\psi) - \alpha'_N{}^{(t)}(\psi) \right| \leq k \mathcal{W}_1(\alpha_N^{(t)}, \alpha'_N{}^{(t)}) \leq k \mathcal{W}_2(\alpha_N^{(t)}, \alpha'_N{}^{(t)}). \quad (85)$$

We denote by  $M_q(\rho)$  the  $q$ -th moment  $\int_{\mathcal{X}} |x|^q \rho(dx)$  of a probability measure  $\rho$  defined on  $\mathcal{X}$ , and assume that  $\mathcal{X}$  contains the origin  $\mathbf{0}_{d_x}$ , otherwise we can add a constant to the diameter  $\mathfrak{d}$ , such that

$$|x|^q \leq \mathfrak{d}^q = \left( \tau \|\psi\|_{\infty} \right)^q, \quad (86)$$

where  $\tau = \frac{\mathfrak{d}}{\|\psi\|_{\infty}}$ . Assume  $M_q(\alpha'_N{}^{(t)}) < \infty$  for some  $q > p = 2$ , following Theorem 1 of [90] and notice that  $|\alpha'_N{}^{(t)}(\psi) - \alpha'_N{}^{(t)}(\psi)| \leq 2\|\psi\|_{\infty}$ , we have that for all  $N \geq 1$ :

$$\mathbb{E} \left[ \left| \alpha'_N{}^{(t)}(\psi) - \alpha'_N{}^{(t)}(\psi) \right|^2 \right] \quad (87)$$

$$\leq 2k \|\psi\|_{\infty} \mathbb{E} \left[ \mathcal{W}_2(\alpha_N^{(t)}, \alpha'_N{}^{(t)}) \right] \quad (88)$$

$$\leq 2k \|\psi\|_{\infty} \sqrt{C_1 M_q^{p/q}(\alpha'_N{}^{(t)}) \mathcal{H}(N, p, d_{\mathcal{X}}, q)} \quad (89)$$

$$\leq 2k \|\psi\|_{\infty} \sqrt{C_1 \tau^p \|\psi\|_{\infty}^p \mathcal{H}(N, p, d_{\mathcal{X}}, q)} \quad (90)$$

$$\leq 2k \sqrt{\mathcal{Q}} \|\psi\|_{\infty}^2 \quad (91)$$

$$\leq C_1 \|\psi\|_{\infty}^2 \quad (92)$$

where  $C_1 := C_1(k, \tau, N, p, d_{\mathcal{X}}, q) := 2k \sqrt{\mathcal{Q}(\tau, N, p, d_{\mathcal{X}}, q)}$ ,  $p$  is the order of the Wasserstein distance ( $p = 2$  in this case),  $C_1$  is a constant depending only on  $p$ ,  $d$ ,  $q$ ,  $\mathcal{Q} := \mathcal{Q}(\tau, N, p, d_{\mathcal{X}}, q) := C_1 \tau^p \mathcal{H}(N, p, d_{\mathcal{X}}, q)$ , and  $\mathcal{H}(N, p, d_{\mathcal{X}}, q)$  is defined as

$$\mathcal{H}(N, p, d_{\mathcal{X}}, q) = \begin{cases} N^{-1/2} + N^{-(q-p)/q} & \text{if } p > d_{\mathcal{X}}/2 \\ & \text{and } q \neq 2p, \\ N^{-1/2} \log(1+N) + N^{-(q-p)/q} & \text{if } p = d_{\mathcal{X}}/2 \\ & \text{and } q \neq 2p, \\ N^{-p/d_{\mathcal{X}}} + N^{-(q-p)/q} & \text{if } p \in (0, d_{\mathcal{X}}/2) \\ & \text{and } q \neq d_{\mathcal{X}}/(d_{\mathcal{X}} - p), \end{cases} \quad (93)$$

For the second term in Eq. (83), by Assumption V.3, V.4 and Proposition B.1:

$$\left| \alpha'_N{}^{(t)}(\psi) - \beta_N^{(t-1)} f(\psi) \right| \quad (94)$$

$$\leq \eta \left| \tilde{\beta}_{N,\epsilon}^{(t-1)}(\psi) - \beta_N^{(t-1)}(\psi) \right| \quad (95)$$

$$\leq \sqrt{2} \eta k \left( 2\lambda^{1/2} \mathcal{E}^{1/2} [\mathfrak{d} + \mathcal{E}]^{1/2} \right.$$

$$\left. + \max\{\lambda, 1\} \left[ \mathcal{W}_2 \left( \alpha_N^{(t-1)}, \alpha'_N{}^{(t-1)} \right) + \mathcal{W}_2 \left( \beta_N^{(t-1)}, \frac{\omega \alpha'_N{}^{(t-1)}}{\alpha'^{(t-1)}(\omega)} \right) \right] \right) \quad (96)$$

$$\leq \sqrt{2} \eta k \left( 2\lambda^{1/2} \mathcal{E}^{1/2} [\mathfrak{d} + \mathcal{E}]^{1/2} \right.$$

$$\left. + \max\{\lambda, 1\} \left[ (1+\zeta) \mathcal{W}_2 \left( \alpha_N^{(t-1)}, \alpha'_N{}^{(t-1)} \right) \right] \right), \quad (97)$$

where  $\lambda$  is the Lipschitz constant of the optimal transport map  $\mathbf{T}(\cdot) : \mathcal{X} \rightarrow \mathcal{X}$  between  $\alpha'_N{}^{(t-1)}$  and  $\frac{\omega \alpha'_N{}^{(t-1)}}{\alpha'^{(t-1)}(\omega)}$ , and  $\mathcal{E} := \mathcal{W}_2 \left( \alpha_N^{(t-1)}, \alpha'_N{}^{(t-1)} \right) + \mathcal{W}_2 \left( \beta_N^{(t-1)}, \frac{\omega \alpha'_N{}^{(t-1)}}{\alpha'^{(t-1)}(\omega)} \right) +$



$\sqrt{2\epsilon \log(N)}$ . Again following Theorem 1 of [90], assume  $M_q(\alpha'_N{}^{(t-1)}) < \infty$  for  $q > p = 2$ , we have that for all  $N \geq 1$ :

$$\mathbb{E}[\mathcal{E}] \quad (98)$$

$$:= \mathbb{E} \left[ \mathcal{W}_2 \left( \alpha_N^{(t-1)}, \alpha'_N{}^{(t-1)} \right) + \mathcal{W}_2 \left( \beta_N^{(t-1)}, \frac{\omega \alpha'_N{}^{(t-1)}}{\alpha'_N{}^{(t-1)}(\omega)} \right) + \sqrt{2\epsilon \log(N)} \right] \quad (99)$$

$$\leq \mathbb{E} \left[ (1 + \zeta) \mathcal{W}_2 \left( \alpha_N^{(t-1)}, \alpha'_N{}^{(t-1)} \right) + \sqrt{2\epsilon \log(N)} \right] \quad (100)$$

$$\leq (1 + \zeta) \mathbb{E} \left[ \mathcal{W}_2 \left( \alpha_N^{(t-1)}, \alpha'_N{}^{(t-1)} \right) \right] + \mathbb{E} \left[ \sqrt{2\epsilon \log(N)} \right] \quad (101)$$

$$\leq (1 + \zeta) \|\psi\|_\infty \sqrt{C_1 \tau^p \mathcal{H}(N, p, d_{\mathcal{X}}, q)} + \mathbb{E} \left[ \sqrt{2\epsilon \log(N)} \right], \quad (102)$$

and

$$\mathbb{E}[\mathcal{E}^2] \leq \mathbb{E} \left[ \mathcal{E} (2\mathfrak{d} + \sqrt{2\epsilon \log(N)}) \right] \quad (103)$$

$$= 2\mathfrak{d} \mathbb{E}[\mathcal{E}] + \mathbb{E} \left[ \mathcal{E} (\sqrt{2\epsilon \log(N)}) \right] \quad (104)$$

$$\leq 2\mathfrak{d} \mathbb{E}[\mathcal{E}] + \mathbb{E} \left[ 2\mathfrak{d} \sqrt{2\epsilon \log(N)} + 2\epsilon \log(N) \right] \quad (105)$$

Let  $\epsilon_N = o(1/\log N)$  such that  $\mathbb{E} \left[ \sqrt{2\epsilon \log(N)} \right] = 0$  and  $\mathbb{E} \left[ 2\epsilon \log(N) \right] = 0$ , we now have:

$$\mathbb{E}[\mathcal{E}] \leq (1 + \zeta) \|\psi\|_\infty \sqrt{\mathcal{Q}}, \quad (106)$$

$$\mathbb{E}[\mathcal{E}^2] \leq 2\mathfrak{d}(1 + \zeta) \|\psi\|_\infty \sqrt{\mathcal{Q}}. \quad (107)$$

Therefore we have that:

$$\mathbb{E} \left[ \left| \alpha'_N{}^{(t)}(\psi) - \beta_N^{(t-1)} f(\psi) \right| \right] \quad (108)$$

$$\leq \mathbb{E} \left[ \sqrt{2\eta} k \left( 2\lambda^{1/2} \mathcal{E}^{1/2} [\mathfrak{d} + \mathcal{E}]^{1/2} + \max\{\lambda, 1\} \left[ (1 + \zeta) \mathcal{W}_2 \left( \alpha_N^{(t-1)}, \alpha'_N{}^{(t-1)} \right) \right] \right) \right] \quad (109)$$

$$\leq \sqrt{2\eta} k \mathbb{E} \left[ 2\lambda^{1/2} (\mathfrak{d}\mathcal{E} + \mathcal{E}^2)^{1/2} + \max\{\lambda, 1\} (1 + \zeta) \|\psi\|_\infty \sqrt{C_1 \tau^p \mathcal{H}(N, p, d_{\mathcal{X}}, q)} \right] \quad (110)$$

$$\leq \sqrt{2\eta} k \left( 2\lambda^{1/2} \sqrt{\mathbb{E}[\mathfrak{d}\mathcal{E} + \mathcal{E}^2]} + \max\{\lambda, 1\} (1 + \zeta) \|\psi\|_\infty \sqrt{C_1 \tau^p \mathcal{H}(N, p, d_{\mathcal{X}}, q)} \right) \quad (111)$$

$$\leq \sqrt{2\eta} k \|\psi\|_\infty \left( 2\sqrt{3\lambda(1 + \zeta)\tau\sqrt{\mathcal{Q}}} + \max\{\lambda, 1\} (1 + \zeta) \sqrt{\mathcal{Q}} \right) \quad (112)$$

In addition, notice that  $|\alpha'_N{}^{(t)}(\psi) - \beta_N^{(t-1)} f(\psi)| \leq 2\|\psi\|_\infty$ , therefore,

$$\mathbb{E} \left[ \left| \alpha'_N{}^{(t)}(\psi) - \beta_N^{(t-1)} f(\psi) \right|^2 \right] \quad (113)$$

$$\leq 2\|\psi\|_\infty \mathbb{E} \left[ \left| \alpha'_N{}^{(t)}(\psi) - \beta_N^{(t-1)} f(\psi) \right| \right] \quad (114)$$

$$\leq 2\sqrt{2} k \eta \left( 2\sqrt{3\lambda(1 + \zeta)\tau\sqrt{\mathcal{Q}}} + \max\{\lambda, 1\} (1 + \zeta) \sqrt{\mathcal{Q}} \right) \|\psi\|_\infty^2 \quad (115)$$

$$= \mathcal{C}_2 \|\psi\|_\infty^2, \quad (116)$$

where  $\mathcal{C}_2 := \mathcal{C}_2(\lambda, k, \eta, \zeta, \tau, N, p, q, d_{\mathcal{X}}) := 2\sqrt{2} k \eta \left( 2\sqrt{3\lambda(1 + \zeta)\tau\sqrt{\mathcal{Q}}} + \max\{\lambda, 1\} (1 + \zeta) \sqrt{\mathcal{Q}} \right)$ .

From Eq. (92) and Eq. (116), we have that

$$\mathbb{E} \left[ \left( \alpha_N^{(t)}(\psi) - \beta_N^{(t-1)} f(\psi) \right)^2 \right] \quad (117)$$

$$\leq \mathbb{E} \left[ \left( \alpha_N^{(t)}(\psi) - \alpha'_N{}^{(t)}(\psi) \right)^2 + \left( \alpha'_N{}^{(t)}(\psi) - \beta_N^{(t-1)} f(\psi) \right)^2 \right] \quad (118)$$

$$\leq 2\mathcal{C}_1 \|\psi\|_\infty + 2\mathcal{C}_2 \|\psi\|_\infty \quad (119)$$

$$\leq \mathcal{C} \|\psi\|_\infty^2, \quad (120)$$

where  $\mathcal{C} := \mathcal{C}(\lambda, k, \eta, \zeta, \tau, N, p, q, d_{\mathcal{X}}) = 4k\sqrt{\mathcal{Q}} + 4\sqrt{2} k \eta \left( 2\sqrt{3\lambda(1 + \zeta)\tau\sqrt{\mathcal{Q}}} + \max\{\lambda, 1\} (1 + \zeta) \sqrt{\mathcal{Q}} \right)$ . Besides, for large enough  $N$  and  $d_{\mathcal{X}}$  such that  $\mathcal{Q} \leq \sqrt{\mathcal{Q}} \leq \sqrt[4]{\mathcal{Q}}$  and  $\mathcal{H}(N, p, d_{\mathcal{X}}, q) = N^{-p/d_{\mathcal{X}}} + N^{-(q-p)/q} \leq 2N^{-p/d_{\mathcal{X}}}$  with  $p = 2$ , we also have that:

$$\mathbb{E} \left[ \left( \alpha_N^{(t)}(\psi) - \beta_N^{(t-1)} f(\psi) \right)^2 \right] \quad (121)$$

$$\leq \|\psi\|_\infty^2 \left[ 4k\sqrt{\mathcal{Q}} + 4\sqrt{2} k \eta \left( 2\sqrt{3\lambda(1 + \zeta)\tau\sqrt{\mathcal{Q}}} \right. \right. \quad (122)$$

$$\left. \left. + \max\{\lambda, 1\} (1 + \zeta) \sqrt{\mathcal{Q}} \right) \right] \quad (123)$$

$$\leq \|\psi\|_\infty^2 \left[ 4k\sqrt[4]{\mathcal{Q}} + 4\sqrt{2} k \eta \sqrt[4]{\mathcal{Q}} \left( 2\sqrt{3\lambda(1 + \zeta)\tau} \right. \right. \quad (124)$$

$$\left. \left. + \max\{\lambda, 1\} (1 + \zeta) \right) \right] \quad (125)$$

$$\leq \tilde{\mathcal{C}} \|\psi\|_\infty^2, \quad (126)$$

where  $\tilde{\mathcal{C}} := \tilde{\mathcal{C}}(\lambda, k, \eta, \mathfrak{d}, \tau, N, p, q, d_{\mathcal{X}}) := 4k\sqrt[4]{2C_1\mathfrak{d}^2} \left( 1 + \sqrt{2\eta} \left( 2\sqrt{3\lambda(1 + \zeta)\tau} + \max\{\lambda, 1\} (1 + \zeta) \right) \right)$ .  $\square$

**Lemma B.5.** *Provided the weight function  $\omega(\cdot) : \mathcal{X} \rightarrow \mathbb{R}$  is upper bounded, for all measurable and bounded function  $\psi(\cdot) : \mathcal{X} \rightarrow \mathbb{R}$ ,*

$$\mathbb{E} \left[ \left| \beta_N^{(t)}(\psi) - \beta'_N{}^{(t)}(\psi) \right|^2 \right] \leq \|\psi\|_\infty^2 \mathbb{E} \left[ \left( \alpha_N^{(t)}(\bar{\omega}) - 1 \right)^2 \right], \quad (127)$$

where  $\bar{\omega}(\cdot) : \mathcal{X} \rightarrow \mathbb{R}$  is defined as  $\bar{\omega}(x) = \frac{\omega(x)}{\alpha^{(t)}(\bar{\omega})}$ , and  $\beta'_N^{(t)} = \frac{\omega \alpha_N^{(t)}}{\alpha^{(t)}(\bar{\omega})}$ .

*Proof.* Notice that

$$\beta_N^{(t)}(\psi) = \frac{\beta'_N^{(t)}(\psi)}{\alpha_N^{(t)}(\bar{\omega})},$$

therefore, we have that

$$\beta_N^{(t)}(\psi) - \beta'_N^{(t)}(\psi) = \beta_N^{(t)}(\psi) \left(1 - \alpha_N^{(t)}(\bar{\omega})\right) \quad (128)$$

$$\leq \|\psi\|_\infty \left(1 - \alpha_N^{(t)}(\bar{\omega})\right). \quad (129)$$

So, we can conclude that

$$\mathbb{E} \left[ \left| \beta_N^{(t)}(\psi) - \beta'_N^{(t)}(\psi) \right|^2 \right] \leq \|\psi\|_\infty^2 \mathbb{E} \left[ \left( \alpha_N^{(t)}(\bar{\omega}) - 1 \right)^2 \right]. \quad (130)$$

□

**Proposition V.1.** For a bounded weight function  $\omega_t(x_t) = p(y_t | x_t; \theta) : \mathcal{X} \rightarrow \mathbb{R}$  and a measurable bounded  $k$ -Lipschitz function  $\psi(\cdot) : \mathcal{X} \rightarrow \mathbb{R}$ , when the regularisation coefficient in entropy-regularised optimal transport resampler  $\epsilon_N = o(1/\log N)$ , there exist constants  $c_t$  and  $c'_t$  such that for  $t \geq 0$

$$\mathbb{E} \left[ \left( \alpha_N^{(t)}(\psi) - \beta^{(t-1)} f(\psi) \right)^2 \right] \leq c_t \frac{\|\psi\|_\infty^2}{N^{1/2d_{\mathcal{X}}}} \quad (131)$$

(replacing  $\beta^{(t-1)} f$  by the initial distribution  $\pi(x_0, \theta)$  at time  $t = 0$  defined in Eq. (1)) and

$$\mathbb{E} \left[ \left( \beta_N^{(t)}(\psi) - \beta^{(t)}(\psi) \right)^2 \right] \leq c'_t \frac{\|\psi\|_\infty^2}{N^{1/2d_{\mathcal{X}}}}, \quad (132)$$

where  $\beta^{(t)}$  and  $\alpha_N^{(t)}$  are respectively defined by Eqs. (54) and (55), and  $f(\cdot)$  is a transition kernel defined by  $p(x_t | x_{t-1}; \theta)$  in Eq. (17).

*Proof.* We prove the above statement by induction. Firstly, Eq. (131) holds at time  $t = 0$  with  $c_1 = 4$ :

$$\mathbb{E}_{x_0^i \stackrel{\text{i.i.d.}}{\sim} \pi} \left[ \left( \frac{1}{N} \sum_{i=1}^N \psi(x_0^i) - \pi(\psi) \right)^2 \right] \quad (133)$$

$$= \text{Var} \left( \frac{1}{N} \sum_{i=1}^N \psi(x_0^i) \right) \quad (134)$$

$$= \frac{1}{N} \text{Var}(\psi(x)) \quad (135)$$

$$= \frac{1}{N} \mathbb{E}_{X \sim \mu} \left[ \left( \psi(x) - \mu(\psi) \right)^2 \right] \quad (136)$$

$$\leq \frac{1}{N} (2\|\psi\|_\infty)^2 \quad (137)$$

$$\leq \frac{4\|\psi\|_\infty^2}{N^{1/2d_{\mathcal{X}}}}. \quad (138)$$

Assume Eq. (131) holds at time  $t \geq 0$ , we have:

$$\begin{aligned} & \beta_N^{(t)}(\psi) - \beta^{(t)}(\psi) \\ &= \left( \beta_N^{(t)}(\psi) - \beta'_N^{(t)}(\psi) \right) + \left( \beta'_N^{(t)}(\psi) - \beta^{(t)}(\psi) \right). \end{aligned} \quad (139)$$

The MSE of the second term in the r.h.s of Eq. (139) can be bounded by applying Eq. (131) to function  $\bar{\omega}\psi$ . The MSE of the first term in the r.h.s of Eq. (139) can be bounded by applying Lemma B.5, then Eq. (131) to function  $\bar{\omega}$  (using the fact that  $\beta^{(t-1)} f(\bar{\omega}) = 1$ ). Therefore

$$\mathbb{E} \left[ \left( \beta_N^{(t)}(\psi) - \beta^{(t)}(\psi) \right)^2 \right] \quad (140)$$

$$\leq 2\mathbb{E} \left[ \left( \beta_N^{(t)}(\psi) - \beta'_N^{(t)}(\psi) \right)^2 \right] + 2\mathbb{E} \left[ \left( \beta'_N^{(t)}(\psi) - \beta^{(t)}(\psi) \right)^2 \right] \quad (141)$$

$$\leq 4c_t \frac{\|\psi\|_\infty^2 \|\bar{\omega}\|_\infty^2}{N^{1/2d_{\mathcal{X}}}}, \quad (142)$$

where we can obtain Eq. (132) with  $c'_t = 4c_t \frac{\|\bar{\omega}\|_\infty^2}{N^{1/2d_{\mathcal{X}}}}$ .

We then prove that Eq. (132) at time  $t-1$  implies Eq. (131) at time  $t$ . Firstly, we have that

$$\alpha_N^{(t)}(\psi) - \beta^{(t-1)} f(\psi) \quad (143)$$

$$= \left( \alpha_N^{(t)}(\psi) - \beta_N^{(t-1)} f(\psi) \right) + \left( \beta_N^{(t-1)} f(\psi) - \beta^{(t-1)} f(\psi) \right). \quad (144)$$

The MSE of the first term in the r.h.s of Eq. (143) can be bounded by applying Lemma B.4, and the MSE of the second term in the r.h.s of Eq. (143) can be bounded by applying Eq. (132) (at time  $t-1$ , replacing  $\psi$  by  $f\psi$ ), therefore we have that Eq. (131) holds:

$$\mathbb{E} \left[ \left( \alpha_N^{(t)}(\psi) - \beta^{(t-1)} f(\psi) \right)^2 \right] \quad (145)$$

$$\leq 2\mathbb{E} \left[ \left( \alpha_N^{(t)}(\psi) - \beta_N^{(t-1)} f(\psi) \right)^2 \right] \quad (146)$$

$$+ 2\mathbb{E} \left[ \left( \beta_N^{(t-1)} f(\psi) - \beta^{(t-1)} f(\psi) \right)^2 \right] \quad (147)$$

$$\leq 2 \left[ \tilde{C} + c'_t \right] \frac{\|\psi\|_\infty^2}{N^{1/2d_{\mathcal{X}}}}. \quad (148)$$

So, Eq. (132) at time  $t-1$  leads to Eq. (131) at time step  $t$  with  $c_t = 2(\tilde{C} + c'_t)$ , where  $\tilde{C}$  is defined by Eq. (80).

To summarise, we have Eq. (131) to hold at time 0, and Eq. (131) at time step  $t$  implies Eq. (132) to hold at time step  $t$ . Then Eq. (132) at time step  $t$  lead to Eq. (131) at time step  $t+1$ , therefore we can conclude that Eq. (131) and Eq. (132) hold for  $\forall t \geq 0$ . □